

Cosmological Constant, Dark Matter, and Electroweak Phase Transition

Daniel Chung and Andrew Long

Department of Physics, University of Wisconsin, Madison, WI 53706

E-mail: danielchung@wisc.edu, ajlong@wisc.edu

Accepting the fine tuned cosmological constant hypothesis, we have recently proposed that this hypothesis can be tested if the dark matter freeze out occurs at the electroweak scale and if one were to measure an anomalous shift in the dark matter relic abundance. In this paper, we numerically compute this relic abundance shift in the context of explicit singlet extensions of the Standard Model and explore the properties of the phase transition which would lead to the observationally most favorable scenario. Through the numerical exploration, we explicitly identify a parameter space in a singlet extension of the standard model which gives order unity observable effects. We also clarify the notion of a temperature dependence in the vacuum energy.

Contents

1. Introduction	2
2. A Brief Review of the Physics of Phase Transitions	4
3. An Analytic Estimate of the Change in the Dark Matter Abundance	9
4. Illustrative Models	17
4.1. Standard Model with Dark Matter	18
4.2. SM Singlet Extension with \mathbb{Z}_2	22
4.3. Generic Single Scalar Model	25
4.4. Singlet Extension with First Order PT	31
5. Conclusion	34
A. Renormalization Scale	36
B. Derivation of Eq. (3.3)	37

C. Difference Between Entropy and Energy Degrees of Freedom	38
D. Derivation of T_{PT}^+, Δs, and $T(a)$	39
E. Derivation of PT induced change in the degree of freedom	41
F. Thermal Effective Potential Details	42
1. Thermal Effective Potential: Standard Model	42
2. Thermal Effective Potential: \mathbb{Z}_2 xSM	44
3. Thermal Effective Potential: Generic Singlet	44
4. Thermal Effective Potential: xSM	46
G. xSM Bounce Calculation	47
Acknowledgments	50
References	50

1. INTRODUCTION

The hypothesis that the cosmological constant (CC) energy density today is a result of a tuning between UV and IR contributions [1, 2] is favored according to some versions of the string landscape proposal (see e.g. [3]). Furthermore, this hypothesis has always been the default assumption in particle physics model building (see e.g. [4, 5]). Unfortunately, this conjecture is notoriously difficult to test with lab experiments, such as those at colliders.

One of the predictions of the tuning hypothesis is that there can be an electroweak scale effective CC in the early universe if there was a phase transition (PT) at that scale. A well-known reason to suspect that there was an electroweak scale PT in the early universe is the thermally supported electroweak symmetry restoration phenomenon in the context of the Standard Model (SM) of particle physics [6, 7]. Hence, if lab experiments, such as particle colliders, can eventually measure the field content and couplings of the scalar sector at the electroweak scale with sufficient accuracy, then one may be able to predict the CC energy density existing at around the time of the PT. Such an energy density would interact with gravity to modify the expansion history of the universe. Indeed, Kolb and Wolfram [8] were one of the first to state that this computable energy density arising from the Standard Model Higgs condensate may have an observationally acceptable yet significant effect

in cosmology.

In a recent paper [9], we proposed that dark matter freeze out can be used to probe PTs, including the properties of such a computable CC, through its effect on the expansion rate of the universe during freeze out. Such an idea is abstractly very similar to the well known big bang nucleosynthesis idea, as well as generic particle probes of cosmology (see e.g. [10–14]). In particular, if a weakly interacting massive particle (WIMP) dark matter candidate is discovered with a mass of the order of TeV, then its freeze out dynamics would be sensitive to the value of the CC during the electroweak scale PT at a temperature of the order of 100 GeV. Therefore accurate measurements of the dark matter and scalar sector properties will, in principle, make possible a lab test of the tuning of the CC. More accurately, what is being tested is the absence of self-tuning mechanisms and/or modified gravitational theories [15–27] that would eliminate or significantly change the effects of vacuum energy during a PT.

For non-first order PTs, it was found that the shift in the relic abundance due to the CC energy density effects is suppressed by $\Delta n_X/n_X = O(g_E^{-1})$ where g_E is the number of relativistic degrees of freedom contributing to the energy density. For first order PTs, it was found that this fractional shift can be generically enhanced by supercooling such that the CC effects can be $O(1)$ with a 1% parameteric tuning. In all cases, the sought after CC “signal” is buried in the dominant “background” coming from the adiabatic change in the number of degrees of freedom and possibly the entropy release near the time of the dark matter freeze out. The adiabatic change in the number of degrees of freedom and the vacuum energy effect tend to increase the relic density today while the entropy production effect decreases the relic density.

The purpose of this paper is to complement the previous short paper [9] in several ways:

1. Present an explicit singlet extension of the Standard Model (SM) that gives a large supercooling with a first order PT at the electroweak scale.
2. Clarify the notion of how an effective vacuum energy (which is Lorentz invariant in the flat space limit) can depend on temperature (which manifestly breaks Lorentz invariance).
3. Compare numerical results with analytic results presented in [9].
4. Provide relevant technical details that were left out in [9] to aid future research efforts in this direction.

In addition to giving a generic singlet scalar model coupled to a Dirac fermion that gives a significant

supercooling, we analyze xSM, i.e. a real singlet coupled to the SM, and identify a parametric region in which significant supercooling occurs. As anticipated in [9], an $O(10^{-2})$ tuning is sufficient to induce an $O(1)$ supercooling effect on the relic abundance.

The order of presentation is as follows. In Section 2 we review the physics of PTs and focus on the myriad ways in which a PT may impact dark matter freeze out. We clarify the notion of a temperature dependence of vacuum energy density in this section. In Section 3 we analytically compute the fractional shift of the relic abundance $\delta n_X(t_0)$ due to an electroweak scale PT in the limit in which the PT represents a small perturbation to the usual freeze out. In Section 4 we compute the relic abundance deviation in the SM and minimal singlet extensions (both supplemented by a generic dark matter which is assumed to play a negligible role in determining the properties of the PT). In Section 5 we conclude with a summary and suggestions for future work. An extensive set of appendices detail technicalities useful for the material presented in the body of the paper.

Throughout the paper, we assume a flat Friedmann-Robertson-Walker (FRW) metric, $ds^2 = dt^2 - a^2(t)|d\mathbf{x}|^2$, and use the reduced Planck mass $M_p \approx 2.4 \times 10^{18}$ GeV.

2. A BRIEF REVIEW OF THE PHYSICS OF PHASE TRANSITIONS

In this section, we review the physical features that accompany a cosmological PT. Each of these features modifies one of the relationships, $\rho \sim T^4$, $T \sim a^{-1}$, or $\langle\sigma v\rangle = \langle\sigma v\rangle(T)$, which are assumed in the usual freeze out calculation. One of the topics discussed in this section is how to understand the thermal dependence of vacuum energy, which a priori is an oxymoron. Readers interested in mostly the phenomenology can skip to the next section.

The standard cosmological model assumes an expanding FRW universe which leads to the temperature of the relativistic species in the universe decreasing as a function of time except during the time periods when entropy is generated. As the temperature decreases, there may exist critical temperatures at which the thermodynamic quantities are not analytic as a function of temperature and/or the symmetries of the effective Lagrangian governing the dynamical degrees of freedom changes. Following the typical convention in the literature, we refer to the passages through these critical temperatures as PTs.

In order to calculate thermodynamic quantities in the system described above, we will use the thermal effective potential (see [28] for a review). The thermal effective potential $V_{\text{eff}}(\phi_c, T)$, derived from Legendre transforming the partition function coupled to external sources, represents the free

energy density of the plasma at temperature T dynamically interacting with a homogeneous scalar field background ϕ_c which may affect the masses and interactions of particles in the plasma. A local minimum $\phi_c = v(T)$ is called the thermal vacuum, and PTs occur near critical temperatures T_c which will be defined more precisely below.¹

The critical temperature T_c in the case of what is conventionally referred to as a first order PT is defined by the existence of two or more degenerate minima $\phi = v(T_c)$ existing for the thermal effective potential $V_{\text{eff}}(\phi, T_c)$. In such cases, we refer to the vacuum of the universe just prior to the PT as $v^{(s)}(T)$ (where the “s” superscript denotes “symmetric” vacuum) whether or not there is a symmetry in the thermal effective potential prior to the PT. The vacuum solution after the first order PT is referred to as $v^{(b)}(T)$ where “b” denotes “broken.” A non-first order PT (sometimes loosely referred to as a second order PT) is characterized by a single continuous function $v(T)$ before and after the PT: i.e. $v^{(b)}(T_c) = v^{(s)}(T_c)$. Even in such situations, it is sometimes useful to define $v^{(s)}(T)$ to be the vacuum before the PT whenever there is a restored symmetry prior to the PT. The quantity $v^{(s)}(T)$ can then be taken as an order parameter associated with spontaneous symmetry breaking.

The thermal vacua $v^{(s/b)}(T)$ can be obtained from summing up thermal tadpole corrections obtained from expanding perturbatively about the zero temperature vacua $v^{(s/b)}(0)$. Despite the suggestive notation of the thermally shifted vacuum $v^{(s/b)}(T)$, the resummation of tadpoles is nothing more than a reorganization of perturbation theory, and the vacuum energy represented by the Lorentz-invariant part of the energy-momentum tensor, is not shifted by the manifestly Lorentz-noninvariant thermal tadpoles. Note that symmetry restoration cannot be inferred from the thermal tadpole resummation alone since the thermal perturbation theory breaks down when the perturbations are expanded about the inflection points of the effective potential.

Let us now establish some more notation for the quantities introduced above. The thermal effective potential and $v^{(s/b)}(T)$ can be used to construct the thermodynamic quantities

$$\mathcal{F}^{(s/b)}(T) = V_{\text{eff}}(v^{(s/b)}(T), T) \quad (2.1a)$$

$$s^{(s/b)}(T) = -\frac{d}{dT} \mathcal{F}^{(s/b)} \quad (2.1b)$$

$$\rho^{(s/b)}(T) = \mathcal{F}^{(s/b)} + T s^{(s/b)} \quad (2.1c)$$

representing the free energy density \mathcal{F} , entropy density s , and energy density ρ in the symmetric and

¹ We will leave out the adjective “thermal” in “thermal vacuum” whenever no confusion should arise.

broken phases. A typical PT occurs as the universe cools, and the free energy of the broken phase, in which the entropy and energy densities are high, drops below the free energy of the symmetric phase, in which the entropy and energy densities are low. It will be useful to define the critical temperature of the PT T_c by

$$\mathcal{F}^{(s)}(T_c) = \mathcal{F}^{(b)}(T_c), \quad (2.2)$$

but note that the PT may not actually occur until a much lower temperature if the symmetric phase experiences supercooling. The PT is accompanied by a number of physical features, which we will outline in the remainder of this section and which each have an impact on dark matter freeze out.

The first feature that we would like to discuss is the vacuum energy associated with the PT. We assume that the energy density $\rho^{(s/b)}(T)$ can be partitioned into the energy associated with the plasma and the energy associated with the condensate (i.e. the vacuum energy with an effective equation of state of -1), and we define the latter as

$$\rho_{cc}^{(s/b)}(T) \equiv V_{\text{eff}}(v^{(s/b)}(T), 0) \quad (2.3)$$

which has an observable consequence when coupled to gravity. This equation is artificial because the vacuum energy cannot be rigorously separated from the particle energy with which it is associated for most of the states populating the density matrix. Nonetheless, it is useful because it captures the CC type of contribution (i.e. negative equation of state contribution) to the energy-momentum tensor.

Note that flat space thermal corrections to the zero temperature effective potential cannot generate Lorentz invariant contributions to the energy-momentum tensor because temperature T dependent quantities are not Lorentz invariant. Since the CC contribution to the energy-momentum tensor in the flat space limit is Lorentz invariant, one may wonder whether Eq. (2.3) is valid since it implies that thermal tadpoles are contributing to the vacuum energy. Furthermore, the fact that the effective vacuum energy takes on a continuum of values while the only non-perturbatively stable vacuum state is at $v^{(b)}(0)$ (which we will assume to be associated with negligible vacuum energy) also leads one to be suspicious of Eq. (2.3).

To semi-quantitatively resolve this puzzle, one notes that near the time of the PT, there are $A \leftrightarrow B$ processes in equilibrium where A and B schematically correspond to states of the form $|\text{particles} + \text{vacuum energy}\rangle$ and $|\text{particles}\rangle$, respectively. These transitions are mediated by non-perturbative processes since they are vacuum changing processes. Classically, the plasma (when

these transitions are efficient) is approximately described by inhomogeneous solutions in Minkowski space. This can easily be characterized by computing for example the thermal two-point function.

The equation of state for such a plasma in the classical approximation corresponds to neither that of quantum expectation values with respect to states A nor B , but is a mixture which from the quantum perspective depends on the non-perturbative transition operators as well as the relative statistical and/or coherent weighting of A and B type of states. The incoherent aspect of this mixture is what the T dependence of Eq. (2.3) reflects.² To corroborate this picture, one can easily solve classical equations of motion in models with spontaneous symmetry breaking to obtain *inhomogeneous background* field solutions which have an inhomogeneous equation of state. Since the Friedmann equation (which is the only gravitational probe we will be concerned in this paper) approximately describes the gravitational response to the spatial average of the energy-momentum tensor, one can spatially average the energy density and the pressure. This leads to an effectively homogeneous energy density and pressure which is approximately the same as that due to particles plus a vacuum condensate energy density. The resulting effective vacuum condensate energy density is somewhere between $V_{\text{eff}}(v^{(s)}(0), 0)$ and $V_{\text{eff}}(v^{(b)}(0), 0)$, justifying the diagnostic quantity defined by Eq. (2.3).

To renormalize the CC, we impose the tuning condition

$$\rho_{cc}^{(b)}(T = 0) = 0, \quad (2.4)$$

which states that the vacuum energy density today is on the order of the meV^4 dark energy density [29, 30] and negligible as compared to the PT scale. Hence, we will refer to $\rho_{cc}^{(s/b)}(T)$ as the “effective CC energy density.” With this normalization, the CC energy density before a PT at scale M will typically be

$$\rho_{cc}^{(s)}(T \gtrsim M) \sim M^4, \quad (2.5)$$

which can be measured, in principle, by gravitational probes such as the Hubble expansion rate and its impact on dark matter freeze out.³ Any self-tuning/modified-gravity mechanism which

² Note also unlike in flat spacetime, there are IR cutoffs associated with the expansion rate H for a single causal domain during the PT and H_0 associated with the presently observable universe. The former scale H is also associated with one of the scales at which quasi-equilibrium assumption breaks down.

³ Although an in depth discussion of UV sensitivity of the CC is beyond the scope of this paper, one should keep in mind that using Eq. (2.4) as a quantum renormalization condition leads to Eq. (2.5) as a prediction only if assumptions about analyticity of the effective potential as well as Lorentz invariance structure of the UV cutoff is assumed.

decouples the vacuum energy or significantly modifies the vacuum energy effect on gravity on a time scale shorter than that of the expansion scale will have an effective $\rho_{cc}^{(s)}$ significantly different from Eq. (2.5). It would be interesting in future studies to compare various self-tuning/modified gravity models which may have non-trivial time dependence in the effective vacuum energy different from that in this paper.

The second PT feature is the decoupling of heavy degrees of freedom which become non-relativistic after the PT and cause the number of relativistic species, denoted here as g , to decrease. This has two consequences for the dark matter freeze out calculation. First, the energy density of the plasma $\rho \sim gT^4$ and Hubble expansion rate $H \sim \sqrt{\rho}$ decrease more rapidly than usual after the PT. Second, since temperature is related to the FRW scale factor by entropy conservation, which gives $T \sim g^{-1/3}a^{-1}$, the temperature decreases less rapidly than usual after the PT. To estimate the magnitude of the effect on dark matter freeze out, consider the SM electroweak PT at $T \sim 100$ GeV and suppose that freeze out occurs at the same temperature. Then during the residual annihilation stage of freezeout, which lasts until $T \sim 10$ GeV, g will decrease by approximately 20% corresponding to the decoupling of the top, Higgs, and massive gauge bosons. In the usual freeze out calculation, changes in g are neglected, because freeze out occurs much later than the electroweak PT when g is insensitive to T . When we arrange for the two events to occur at the same scale, g decreases significantly and can have a large effect on the relic abundance.

The third feature is related to the coupling between the PT sector and the rest of the particle physics model. As the phase changes at the PT, in general the masses and interactions of particles in the plasma can change as well. In particular, it is possible for the scalar field to couple to dark matter in such a way that the dark matter's mass and/or annihilation cross section is different in the symmetric and broken phases. This scenario, studied by [31, 32], may allow dark matter to rethermalize and can have a significant effect on the relic abundance.

If the PT is of the first order, then it possesses a number of additional features. A first order PT can be divided into two stages. The first stage, known as supercooling, occurs while the universe remains in the symmetric phase after it has become metastable at $T \approx T_c$. As the temperature decreases and the CC energy density remains approximately constant, the total energy density can deviate from the standard $\rho \sim T^4$ scaling (i.e., first feature above). Supercooling ends when it becomes energetically favorable for bubbles of the broken phase to nucleate. Determining the temperature T_{PT}^- at which bubble nucleation begins requires one to solve for the non-perturbative bounce solution and evaluate the decay rate of the metastable phase [33]. During the second stage,

known as reheating, the expanding bubbles release an energy density

$$\Delta\rho_{\text{ex}} = \rho_{cc}^{(s)}(T_{PT}^-) - \rho_{cc}^{(b)}(T_{PT}^+) \quad (2.6)$$

which is converted into radiation and heats the gas from T_{PT}^- before the PT to $T_{PT}^+ > T_{PT}^-$ after the PT. We assume that reheating occurs rapidly as compared with the expansion rate of the universe⁴, which allows us to treat reheating as an abrupt process at time t_{PT} when $a = a_{PT}$. Reheating is accompanied by a non-adiabatic entropy increase. This entropy growth modifies the relationship between temperature and the FRW scale factor in such a way that the universe is relatively larger for a given temperature. As a result, the dark matter number density undergoes a longer period of dilution and the relic abundance can be significantly smaller [35]. Finally, just as massive species can adiabatically decouple after the electroweak PT occurs, heavy particles can undergo a non-adiabatic decoupling at the time of a first order PT if they abruptly acquire a mass $m \gtrsim T_{PT}$.

3. AN ANALYTIC ESTIMATE OF THE CHANGE IN THE DARK MATTER ABUNDANCE

In this section, we estimate the change in the dark matter relic abundance due to the presence of a PT, and the CC energy density in particular, during freeze out. Our final result is the fractional deviation of the relic abundance, denoted $\delta n_X(t_0)$ and given by Eq. (3.44), in which we have linearized in the various effects of the PT on freeze out. Although most of the results in this section have already been presented in [9], we repeat some of the results for self-containedness as well as serving as introduction for more complete results such as Eqs. (3.46) and (3.47). The main point of this section is to present a formalism to understand analytically the effects outlined in Sec. 3.

Throughout the calculation, we will take a as the independent variable and rewrite functions of temperature using $T = T(a)$ given by Eq. (D.12). In particular, we will assume that freeze out occurs at a temperature $T_f = T(a_f)$ before the PT at $a = a_{PT}$. Since all of the thermodynamic quantities depend on the phase of the system which changes at $a = a_{PT}$, the formulas in this section would become unnecessarily obscure if we persisted in writing all the (s/b) superscripts and distinguishing the $a < a_{PT}$ and $a > a_{PT}$ cases. Therefore, we introduce the following shorthand.

⁴ A third stage, known as phase coexistence, can occur if a large latent heat is released by the expanding bubbles and the plasma is reheated to the point where the pressure gradient across the bubble wall vanishes [34]. Subsequently, the bubbles expand only insofar as the universe expands, and the PT completes on a time scale $t \sim H^{-1}$. Typically, this stage does not occur during an electroweak-scale PT because the number of relativistic species $O(100)$ is too many to allow for sufficient reheating.

Whenever a temperature-dependent function $F^{(s/b)}(T)$ appears without the (s/b) superscript, the intended meaning is

$$F(a) = \begin{cases} F^{(s)}(T(a)) & a < a_{PT} \\ F^{(b)}(T(a)) & a > a_{PT} \end{cases}. \quad (3.1)$$

In particular, one always has $F(a_f) = F^{(s)}(T_f)$ since $a_f < a_{PT}$ by assumption.

We calculate the thermal relic abundance of dark matter by integrating the thermally averaged Boltzmann equation,

$$\frac{1}{a^3} \frac{d}{dt} (a^3 n_X) = -\langle \sigma v \rangle (n_X^2 - n_X^{\text{eq}2}), \quad (3.2)$$

over the era of residual annihilations from freeze out at $a = a_f$ until today. Subject to general assumptions (see Appendix B for more details), we obtain

$$n_X(t_0) = \left(\int_0^{\ln a_0/a_f} \frac{d \ln(a/a_f)}{H} \langle \sigma v \rangle \frac{a_0^3}{a^3} \right)^{-1} \quad (3.3)$$

for the number density of dark matter today at $a = a_0$ and $t = t_0$. In this expression, the quantities that will be affected by the PT are the Hubble expansion rate $H(a)$, the thermally averaged cross section $\langle \sigma v \rangle(a)$, and the dilution number since the time of the freeze out to today a_0/a_f , which is related to $T(a)$. As a fiducial reference value, we also calculate the “usual” relic abundance $n_X^{(U)}(t_0)$ by assuming that the PT does not occur, but instead that the universe remains radiation dominated and has the standard scaling relations

$$H^{(U)} \sim a^{-2}, \quad \langle \sigma v \rangle^{(U)} = \langle \sigma v \rangle(T(a)), \quad \text{and} \quad T^{(U)} \sim a^{-1} \quad (3.4)$$

throughout freeze out. We define the relic abundance fractional deviation as

$$\delta n_X(t_0) = \frac{n_X(t_0)}{n_X^{(U)}(t_0)} - 1 \quad (3.5)$$

and expect this quantity to depend on the way in which H , $\langle \sigma v \rangle$, and a_0/a_f deviate from the usual freeze out scenario. We will consider each effect in turn.

Before addressing each of the factors in Eq. (3.3), let us discuss the partitioning of energy. The Hubble expansion rate, which appears in Eq. (3.3), is related to the total energy density $\rho^{(s/b)}(T)$. However, we are particularly interested in determining the impact of the effective CC on the calculation of dark matter freeze out. Therefore we will assume that the energy can be partitioned as

$$\rho \approx (\text{particle degrees of freedom} + \text{exotic energy component}). \quad (3.6)$$

In general, the exotic energy component can arise from physics other than the effective CC, such as quintessence (e.g. [13, 14, 36–40]) or late-decaying massive particles (e.g. [41–48]). To maintain a minimal degree of generality throughout our analytic estimates (without accumulating distasteful notational complication), we will parametrize the exotic energy component as $\rho_{\text{ex}} \kappa(a)$. However, since our primary interest is in the case that the exotic energy component represents an effective CC, we will write

$$\rho_{\text{ex}} \kappa(a) = \rho_{\text{cc}}(a) \quad (3.7)$$

where $\rho_{\text{cc}}^{(s/b)}(T)$ is defined by Eq. (2.3), and we have used the shorthand Eq. (3.1). The remaining energy density can be attributed to relativistic particles in the plasma, which we will denote by⁵

$$\rho_R^{(s/b)}(T) = \rho^{(s/b)}(T) - \rho_{\text{cc}}^{(s/b)}(T). \quad (3.8)$$

To connect with a familiar and intuitive notation, we let the functions g_E and g_S be defined implicitly by

$$\rho_R^{(s/b)}(T) = \frac{\pi^2}{30} g_E^{(s/b)}(T) T^4 \quad (3.9)$$

$$s^{(s/b)}(T) = \frac{2\pi^2}{45} g_S^{(s/b)}(T) T^3 \quad (3.10)$$

such that they represent the number of relativistic degrees of freedom at temperature T in either the symmetric or broken phase. As shown in Appendix C, one must have $g_S(T) \neq g_E(T)$ if entropy and energy are to be conserved during the time when a species adiabatically decouples.

Now, we will begin our investigation of the quantities in Eq. (3.3). First, consider the effect on the Hubble expansion rate $H(a)$ which is obtained by solving the Friedmann equation. To do so, we partition the energy as described above and assume that $\rho_{\text{ex}} \ll \rho_R(a_f)$ such that we can treat the CC energy density as a perturbation. With these assumptions, we obtain

$$H(a) = \frac{1}{\sqrt{3}M_p} \sqrt{\rho(a)} \quad (3.11)$$

$$\approx \frac{T^2}{3M_p} \sqrt{\frac{\pi^2}{10} g_E(a)} \left[1 + \frac{1}{2} \frac{\pi^2}{30} \frac{\rho_{\text{ex}} \kappa(a)}{g_E(a) T(a)^4} \right]. \quad (3.12)$$

⁵ Contributions from non-relativistic species are Boltzmann suppressed. Defined in this way, $\rho_R^{(s/b)}$ includes a term proportional to $dv^{(s/b)}/dT$ which arises from the derivative in Eq. (2.1b). This term represents kinetic energy in the scalar field and, strictly speaking, should not be included in ρ_R . Nevertheless, we do not separate out the kinetic term, because it is typically negligible.

where we have used the shorthand Eq. (3.1). During the PT, we can approximate $\kappa(a)$ as

$$\kappa(a) \approx \Theta(a_{PT} - a) + \Theta(a - a_{PT}) \left(1 - \frac{\Delta\rho_{\text{ex}}}{\rho_{\text{ex}}}\right) \kappa_2(a) \quad (3.13)$$

where $\Theta(z)$ is a step function, $\Delta\rho_{\text{ex}} > 0$ is given by Eq. (2.6), and $\kappa_2(a)$ is a function which starts from $\kappa_2(a_{PT}) = 1$ and decreases as fast as

$$\left(\frac{a}{a_{PT}}\right)^{-n_d} \quad (3.14)$$

with $n_d \gtrsim 4$. If $\Delta\rho_{\text{ex}} = 0$, we have a continuous second order transition or a crossover. If $\Delta\rho_{\text{ex}} = \rho_{\text{ex}}$, then the supercooling is sufficiently strong as to end up with no CC energy just after the PT. The step functions represent the fact that the PT occurs with negligible change in the scale factor. With this assumption, Δs and the corresponding change in the temperature become functions of $\Delta\rho_{\text{ex}}$ according to Eq. (D.8) in Appendix D. Finally, the $\Theta(a_{PT} - a)$ term in Eq. (3.13) should, in general, be multiplied by another smooth function unless there is some symmetry fixing $v^{(s)}(T)$, and consequently $\rho_{cc}^{(s)}(T)$, to a particular value in the high energy limit. However, we will neglect this detail in favor of cleaner notation, since the final result will be approximately unchanged.

As discussed in Section 2, particle species start becoming non-relativistic after the (electroweak) PT which causes $g_{E/S}(a)$ to decrease. We will parametrize this decrease by focusing on the (non-)adiabatic decoupling of (N_{PT}) N fermionic dynamical degrees of freedom and write

$$g_{E/S}(a) = g_{E/S}(a_f) - h(a) \quad (3.15)$$

$$h(a) = \frac{7}{8} N_{PT} \Theta(a - a_{PT}) + \frac{7}{8} N f(a) \quad (3.16)$$

where $f(a)$, which rises from 0 to 1, is given by Eq. (E.4). Note that in reality, $h(a)$ is a smooth complicated function (particularly $Nf(a)$), but here we are accounting for the change in the number of degrees of freedom in a physically suggestive approximation. As we will see below, this effect will be one of the dominant “backgrounds” to the “signal” of measuring the effects of the cosmological constant. We treat this effect as a perturbation to linear order, and we estimate the Hubble expansion rate to be

$$H(a) \approx \frac{T(a)^2}{3M_p} \sqrt{\frac{\pi^2}{10} g_E(a_f)} \left[1 - \frac{1}{2} \frac{h(a)}{g_E(a_f)} + \frac{1}{2} \frac{\rho_{\text{ex}} \kappa(a)}{\frac{\pi^2}{30} g_E(a_f) T(a)^4} \right]. \quad (3.17)$$

Writing $T(a)$ using Eq. (D.12) and linearizing further with respect to small quantities, we have

$$H(a) \approx H^{(U)}(a) \left[1 + \frac{\epsilon_1}{2} \left(\frac{a}{a_f}\right)^4 \kappa(a) + \frac{2}{3} \epsilon_2 \Theta(a - a_{PT}) + \frac{1}{6} \epsilon_{31} \Theta(a - a_{PT}) + \frac{1}{6} \epsilon_{32} f(a) \right] \quad (3.18)$$

where

$$H^{(U)}(a) \equiv \frac{T_f^2}{3 M_p \left(\frac{a}{a_f}\right)^2} \sqrt{\frac{\pi^2}{10} g_E(a_f)} \quad (3.19)$$

and

$$\epsilon_1 \equiv \frac{\rho_{\text{ex}}}{\frac{\pi^2}{30} g_E(a_f) T_f^4} = \text{fractional energy of the exotic during freeze out} \quad (3.20a)$$

$$\epsilon_2 \equiv \left(\frac{a_{PT}}{a_f}\right)^3 \frac{\Delta s}{\frac{2\pi^2}{45} g_S(a_f) T_f^3} = \text{fractional entropy increase during PT} \quad (3.20b)$$

$$\epsilon_{31} \equiv \frac{\frac{7}{8} N_{PT}}{g_E(a_f)} = \text{fractional decoupling degrees of freedom during PT} \quad (3.20c)$$

$$\epsilon_{32} \equiv \frac{\frac{7}{8} N}{g_E(a_f)} = \text{fractional decoupling degrees of freedom near freeze out} \quad (3.20d)$$

where Δs , denoting the entropy density change at the time of the PT, is given by Eq. (D.8). Although $H(a)$ appears to vary discontinuously at $a = a_{PT}$, its continuity is ensured by the conservation of energy. At the PT, the CC energy converts into radiation, which generates an entropy but leaves the total energy density fixed (i.e., ϵ_2 compensates for the discontinuity of the ϵ_1 term) because the volume remains approximately constant through the duration of the PT. The fact that H is boosted by ϵ_{31} and ϵ_{32} is intuitive for the following reason. When a particle species becomes non-relativistic, the effective equation of state becomes smaller, such that the energy dilutes less, which in turn leads to a larger expansion rate for the same scale factor. The term ϵ_{31} accounts for the non-adiabatic change in the number of degrees of freedom during the PT, while the term ϵ_{32} accounts for the adiabatic change in the number of degrees of freedom.

Next, consider the change in the cross section due to the PT. We parametrize this effect as

$$\langle \sigma v \rangle = \langle \sigma v \rangle^{(U)} \left(1 - \epsilon_4 \Theta(a - a_{PT})\right) \quad (3.21)$$

where

$$\epsilon_4 \equiv -\frac{\Delta_\sigma}{\langle \sigma v \rangle^{(U)}} \quad (3.22)$$

and Δ_σ is the change in $\langle \sigma v \rangle$ due to the PT. Since the derivation of Eq. (3.3) assumes that the dark matter is decoupled after T_f , we will assume that $\epsilon_4 \gtrsim 0$ in order to prevent re-thermalization due to an increase in the cross section. Hence, we can evaluate Eq. (3.3) by linearizing in the ϵ 's to obtain

$$n_X(t_0) \approx \left(\frac{a_f}{a_0}\right)^3 \left(\int_0^{\ln a_0/a_f} \frac{d \ln a/a_f}{H^{(U)}(a)} \frac{\langle \sigma v \rangle^{(U)}}{(a/a_f)^3} \left[1 + \sum_n \theta_n(a) \epsilon_n\right] \right)^{-1} \quad (3.23)$$

where

$$\begin{aligned} \sum_n \theta_n(a) \epsilon_n = & -\frac{\epsilon_1}{2} \left(\frac{a}{a_f} \right)^4 \kappa(a) - \Theta(a - a_{PT}) \frac{2}{3} \epsilon_2 \\ & - \frac{1}{6} [\epsilon_{31} \Theta(a - a_{PT}) + \epsilon_{32} f(a)] - \epsilon_4 \Theta(a - a_{PT}) \end{aligned} \quad (3.24)$$

implicitly defines the θ_n . Note that the integral is dominated by contributions around $\ln a/a_f = 0$. On the other hand, the $(a_f/a_0)^3$ prefactor should be evaluated with all the g_S changes accounted for, not just the effects around $\ln x = 0$.

Next, let's consider the effects on the a_f/a_0 factor determined by the freeze out condition itself. The freeze out temperature T_f can be solved using [8]

$$\langle \sigma v \rangle n_X^{\text{eq}}(T_f) = C \frac{m_X}{T_f} H(T_f) \quad (3.25)$$

$$n_X^{\text{eq}}(T) \equiv g_X \left(\frac{m_X T}{2\pi} \right)^{3/2} \exp \left(-\frac{m_X}{T} \right) \quad (3.26)$$

where C is an order unity number whose optimum value to reproduce numerical integration is cross section dependent (e.g., $C \approx 2$), g_X counts the real dynamical degrees of freedom of the dark matter, and m_X is the dark matter mass. Evaluating $H(T_f)$ with Eq. (3.18) and assuming freeze out occurs before the PT, Eq. (3.25) becomes

$$\langle \sigma v \rangle g_X \left(\frac{m_X T_f}{2\pi} \right)^{3/2} \exp \left(-\frac{m_X}{T_f} \right) \approx \frac{C m_X T_f}{3M_p} \sqrt{\frac{\pi^2}{10} g_E(a_f)} \left[1 + \frac{\epsilon_1}{2} \right]. \quad (3.27)$$

Although not solvable in closed form, one can linearize in the perturbation again to obtain

$$T_f \approx \frac{m_X}{\ln A} \left[1 + \frac{\epsilon_1}{2} \left(\frac{1}{\ln A} + O((\ln A)^{-2}) \right) \right] \quad (3.28)$$

where

$$A \equiv \frac{g_X 3\sqrt{5} M_p \sqrt{m_X T_f} \langle \sigma v \rangle}{2C \pi^{5/2} \sqrt{g_E(a_f)}} \sim \exp[20] \quad (3.29)$$

for electroweak mass scales. If we assume that there is only one period of entropy production between freeze out and today, and that it occurs at the PT temperature T_{PT} , we can use entropy conservation in the form of Eq. (D.10) to write

$$\frac{a_0}{a_f} = \left(\frac{g_S(a_f)}{g_S(a_0)} \right)^{1/3} \frac{T_f}{T_0} \left[1 + \frac{1}{3} \epsilon_2 \right] \quad (3.30)$$

where T_0 is the temperature today. Combining this with Eq. (3.28), we find

$$\frac{a_0}{a_f} = \left(\frac{a_0}{a_f} \right)^{(U)} \left[1 + \frac{\epsilon_1}{2} \frac{1}{\ln A} + \frac{1}{3} \epsilon_2 \right] \quad (3.31)$$

where

$$\left(\frac{a_0}{a_f}\right)^{(U)} \equiv \left(\frac{g_S(a_f)}{g_S(a_0)}\right)^{1/3} \frac{m_X}{T_0} \frac{1}{\ln A}. \quad (3.32)$$

Putting Eq. (3.31) into Eq. (3.23) results in

$$n_X(t_0) \approx \left(\frac{a_0}{a_f}\right)^{(U)-3} \left[1 - \frac{3\epsilon_1}{2} \frac{1}{\ln A} - \epsilon_2\right] \left(E_1 + \int_0^{\ln(a_0/a_f)^{(U)}} \frac{d \ln a/a_f}{H^{(U)}(a)} \frac{\langle \sigma v \rangle^{(U)}}{(a/a_f)^3} \left[1 + \sum_n \theta_n(a) \epsilon_n\right]\right)^{-1} \quad (3.33)$$

where the endpoint contribution to the integral has been written as

$$E_1 \equiv \frac{\frac{\epsilon_1}{2} \frac{1}{\ln A} + \frac{\epsilon_2}{3}}{H^{(U)}(a_0)} \frac{\langle \sigma v \rangle^{(U)}}{(a_0/a_f)^{(U)3}}. \quad (3.34)$$

The term E_1 is negligible because of the volume dilution factor in its denominator. Linearizing the small factors gives

$$n_X(t_0) \approx n_X^{(U)}(t_0) \left[1 - \frac{3\epsilon_1}{2} \frac{1}{\ln A} - \epsilon_2 - F_u^{-1} \sum_n \tilde{\theta}_n \epsilon_n\right] \quad (3.35)$$

where

$$F_u \equiv \int_0^{\ln(a_0/a_f)^{(U)}} \frac{d \ln a/a_f}{H^{(U)}(a)} \frac{\langle \sigma v \rangle^{(U)}}{(a/a_f)^3} \quad (3.36)$$

$$n_X^{(U)}(t_0) \equiv \left(\frac{a_0}{a_f}\right)^{(U)-3} F_u^{-1} = \text{usual computation of relic abundance} \quad (3.37)$$

$$\tilde{\theta}_n \equiv \int_0^{\ln(a_0/a_f)^{(U)}} \frac{d \ln a/a_f}{H^{(U)}(a)} \frac{\langle \sigma v \rangle^{(U)}}{(a/a_f)^3} \theta_n(a). \quad (3.38)$$

In particular, if we assume an s -wave cross section (i.e., constant $\langle \sigma v \rangle$), we can express $\tilde{\theta}_1$ explicitly as

$$F_u^{-1} \tilde{\theta}_1 \approx -\frac{1}{2} \left[\delta + \frac{(1+3\delta)}{n_d-3} \left(1 - \frac{\Delta \rho_{\text{ex}}}{\rho_{\text{ex}}}\right) \right] \quad (3.39)$$

where we have expanded in $\delta \equiv a_{PT}/a_f - 1 \gtrsim 0$ which represents the delay between freeze out and the PT. The first term in square brackets comes from integrating the CC energy density from a_f to a_{PT} , and the second term comes from integrating the decreasing CC energy density after the PT. This equation shows that if $\frac{\Delta \rho_{\text{ex}}}{\rho_{\text{ex}}} \approx 1$ (large supercooling) there is a suppression of the ϵ_1 effect by a factor of order δ . Although we have linearized in δ along with ϵ_i , terms of the form $\epsilon_i \delta$ are not higher order. The expansion in ϵ_i reflects the fact that we treat the PT as a perturbation, whereas

the expansion in δ is performed merely to simplify the expressions. With the same assumptions, we can evaluate the other $F_u^{-1}\tilde{\theta}_n$ terms:

$$F_u^{-1}\tilde{\theta}_2 \approx -\frac{2}{3}(1-\delta) \quad (3.40)$$

$$F_u^{-1}\tilde{\theta}_{31} \approx -\frac{1}{6}(1-\delta) \quad (3.41)$$

$$F_u^{-1}\tilde{\theta}_{32} \approx -\frac{1}{6} \int_0^{\ln(a_0/a_f)^{(U)}} \frac{d \ln a/a_f}{(a/a_f)^2} f(a) \quad (3.42)$$

$$F_u^{-1}\tilde{\theta}_4 \approx -(1-\delta). \quad (3.43)$$

Hence, for s -wave cross sections, the change in the relic abundance due to small changes made by the PT can be expressed as

$$\delta n_X(t_0) = c_1 \epsilon_1 + c_2 \epsilon_2 + c_{31} \epsilon_{31} + c_{32} \epsilon_{32} + c_4 \epsilon_4 \quad (3.44)$$

where

$$c_1 \equiv \frac{1}{2} \left(\delta + \frac{(1+3\delta)}{n-3} \left(1 - \frac{\Delta \rho_{\text{ex}}}{\rho_{\text{ex}}} \right) \right) - \frac{3}{2} \frac{1}{\ln A} \quad (3.45a)$$

$$c_2 \equiv -\frac{1}{3}(1+2\delta) \quad (3.45b)$$

$$c_{31} \equiv \frac{1}{6}(1-\delta) \quad (3.45c)$$

$$c_{32} \equiv \frac{1}{6} \int_0^{\ln(a_0/a_f)^{(U)}} \frac{d \ln a/a_f}{(a/a_f)^2} f(a) \quad (3.45d)$$

$$c_4 \equiv 1 - \delta. \quad (3.45e)$$

The key point of Eq. (3.44) is that despite the “background” represented by $\epsilon_{n \neq 1}$, the “signal” contained in ϵ_1 can be “measured” and represents a prediction of the hypothesis of a tuned CC. It is a tuned but striking statement, nonetheless. Since this term is central to the rest of our calculation, we have reproduced the so called “CC effect” term here as

$$c_1 \epsilon_1 = \left(\frac{\rho_{\text{ex}}}{\frac{\pi^2}{30} g_E(a_f) T_{PT}^4} \right) \frac{1}{(1+\delta)^4} \left\{ \frac{1}{2} \left[\frac{(1+\delta)^3 - 1}{3} + \frac{(1+\delta)^3}{n_d - 3} \left(1 - \frac{\Delta \rho_{\text{ex}}}{\rho_{\text{ex}}} \right) \right] - \frac{3}{2} \frac{1}{\ln A} \right\} \quad (3.46)$$

without linearizing in δ . We also write the so called “entropy effect” as

$$c_2 \epsilon_2 = -\frac{\delta + \frac{1}{3}}{\delta + 1} \frac{\Delta s}{\frac{2\pi^2}{45} g_S(a_{PT}) T_{PT}^3}. \quad (3.47)$$

Note finally that we can obtain a smooth non-first order PT by taking the limit $\Delta \rho_{\text{ex}} = \epsilon_2 = \epsilon_{31} = \epsilon_4 = 0$.

One should remember that all of the analysis has assumed that the entropy released from the PT (in the case of a first order PT) did not reheat the system to the point that the dark matter rethermalized after freeze out, i.e., $T_{PT}^+ \lesssim T_f$. This provides a lower bound on δ for a given $\Delta\rho_{\text{ex}}$, which can be expressed as

$$\frac{1}{4}\epsilon_{31} + \frac{1}{4} \frac{\Delta\rho_{\text{ex}}}{\frac{\pi^2}{30} g_E(a_f) (T_{PT}^-)^4} \lesssim \delta \quad (3.48)$$

by using Eq. (D.3) and assuming that $f(a_{PT})$ is negligible.

Note also that the range and independence of $\{\epsilon_i, \delta\}$ that is achievable by choosing a beyond the SM Lagrangian is not easy to compute nor to generalize. For example, suppose we want to increase δ while keeping ϵ_1 fixed. To increase δ , we increase a_{PT} more than a_f . Since a_f is mostly determined by the mass of the dark matter m_X while a_{PT} is determined in part by the competition between the thermal mass support and scalar field mass at the field origin, we can keep a_f fixed and increase a_{PT} by decreasing the scalar field mass competing with the thermal support. This, however, typically changes the fractional entropy increase ϵ_2 during the PT. Furthermore, this will change the index n_d (defined in Eq. (3.14)) which depends partly on the flatness of the non-thermal part of the scalar potential. Indeed, we see that if this n_d can be engineered to be as close to 3 as possible (i.e. a flat potential with no thermal particles decoupling), then the ϵ_1 signal can be enhanced. One also sees that in the case of a first order PT, the prediction for the effect of the cosmological constant (i.e., the ϵ_1 piece) depends on $\Delta\rho_{\text{ex}}$ and δ , both of which depend on knowing exactly when the PT occurs. As described in Sec. 2, an accurate computation of this will require a non-perturbative numerical treatment. Hence, the first order PT situation, which can give a larger CC dependent signal, presents an interesting computational challenge of its own.

4. ILLUSTRATIVE MODELS

In this section, we present numerical calculations of $\delta n_X(t_0)$ for various models. This section represents one of the key features of the paper that distinguish it from [9], as discussed in the introduction. For each model we specify the parameters of the scalar sector, which appear in the thermal effective potential $V_{\text{eff}}(\phi_c, T)$, and the parameters of the dark matter sector, m_X , g_X , and $\langle\sigma v\rangle$. We then calculate the relic abundance shift using the methods of Section 3. Most of the numerical results have not been reported previously, and the model dependent analysis of a real singlet extension of the standard model is entirely new.

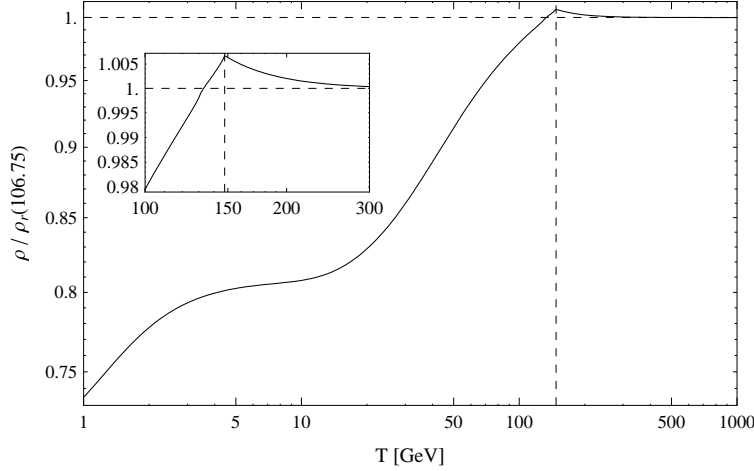


Figure 1: The energy density at the SM PT, $\rho(T) = \rho_{cc}(T) + \rho_R(T)$, relative to the energy density when the entire SM is relativistic, $\rho_r(106.75) \equiv \frac{\pi^2}{30} 106.75 T^4$. Just before the PT at $T \gtrsim 150$ GeV, the energy density grows relative to ρ_r due to the temperature independent CC contribution, $\rho_{cc}(T > T_{PT}) \approx \text{const.}$ After the PT, the top, bottom, Higgs, and massive gauge boson adiabatically decouple causing ρ/ρ_r to drop below one. This adiabatic decoupling is the dominant feature of the SM PT that is relevant for freeze out.

4.1. Standard Model with Dark Matter

We calculate here the relic abundance deviation due to the SM electroweak PT. The qualitative results were already given in [9]. The numerical details that we discuss in this section can be summarized as $\delta n_X(t_0) = O(10^{-3} - 10^{-2})$ with the CC contributing $c_1 \epsilon_1 = O(10^{-4} - 10^{-3})$. With $m_h = 115$ GeV, the largest CC effect occurs for $m_X \approx 4.2$ TeV where $c_1 \epsilon_1 \approx 9.5 \times 10^{-4}$. Our results are summarized in Figures 2 and 3. In this section, we first discuss these figures and then extend the analytic estimate of Section 3, now in the context of a concrete model, to obtain Eq. (4.7), which lets us motivate extensions of the SM that achieve larger $\delta n_X(t_0)$. Some of the qualitative discussion of [9] is reproduced for completeness.

In Appendix F we compute the SM thermal effective potential $V_{\text{eff}}(h_c, T)$ through one-loop order⁶, where $h(x) = \sqrt{2} |H^\dagger H|^{1/2}$ is the radial component of the Higgs field and $h_c = \langle h(x) \rangle$. It is important to point out that the renormalization conditions, given by Eq. (F.5), are chosen such

⁶ It is well known that the one-loop approximation breaks down at the temperature of the SM electroweak PT [49], and that accurate results require lattice calculations [50–52]. However, since the CC contribution already represents perturbative correction to dark matter freeze out, we will neglect higher-order corrections to the PT physics and simply apply the mean field approximation described in Section 2.

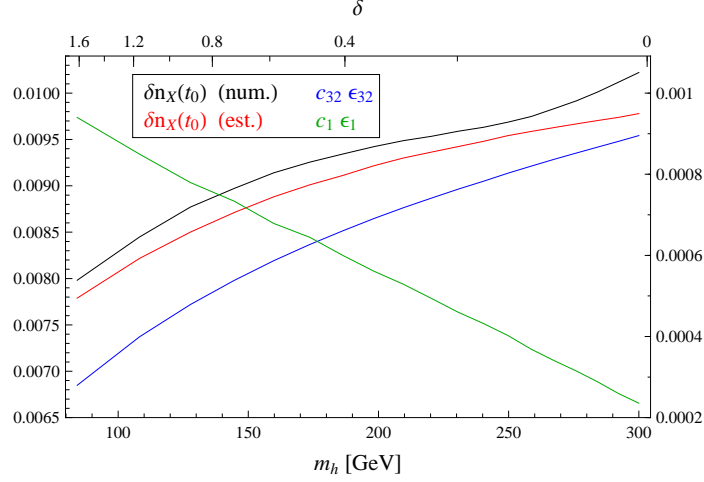


Figure 2: Fractional deviation of the relic abundance due to the SM electroweak PT. The numerical calculation is represented by the black curve, the analytic estimate Eq. (3.44) by the red curve, the CC effect ($c_1 \epsilon_1$ term) by the green curve, and the adiabatic decoupling effect ($c_{32} \epsilon_{32}$ term) by the blue curve. The right axis shows the values of the $c_1 \epsilon_1$ curve only, and the left axis shows the values of the three other curves.

that $V_{\text{eff}}(h_c, 0)$ has a minimum at $v = 246$ GeV where the curvature is m_h^2 and, most importantly the CC is tuned by requiring $V_{\text{eff}}(v, 0) = 0$.

Before discussing the numerical results, it is useful to recall from Section 3 that for a non-first order PT, freeze out is only affected by modifications to the relations $H(T) \propto \sqrt{\rho(T)} \propto T^2$ and $T^3 \propto g_S^{-1} a^{-3} \sim a^{-3}$. These modifications arise when the energy partitioning deviates from radiation domination and the number of relativistic degrees of freedom deviates from a constant value. These deviations can be visualized in Figure 1, where we plot $\rho(T)$ normalized by $\rho_r(106.75) \equiv (\pi^2/30)(106.75) T^4$, the energy density of the SM as if all particles were relativistic. We have taken $m_h = 115$ GeV which gives a PT at $T_{PT} \approx 148$ GeV. As the temperature decreases toward T_{PT} from above, ρ/ρ_r grows to approximately 1.006 due to the presence of the additional CC energy density (i.e., $\lambda v^4/(106.75 T_{PT}^4) \approx 10^{-3}$). Below T_{PT} the massive species decouple, the plasma loses about twenty relativistic degrees of freedom, and ρ/ρ_r decreases to approximately 0.8. This figure illustrates that the adiabatic decoupling has an effect on ρ which is two orders of magnitude larger than that from the CC. Therefore, we expect that the Standard Model electroweak effective CC will have a subdominant effect on the relic abundance as well.

The fractional shift $\delta n_X(t_0)$ is calculated using the perturbative, analytic expressions in Section 3 as well as by solving the Boltzmann equation numerically. In Figure 2 we have plotted $\delta n_X(t_0)$ by

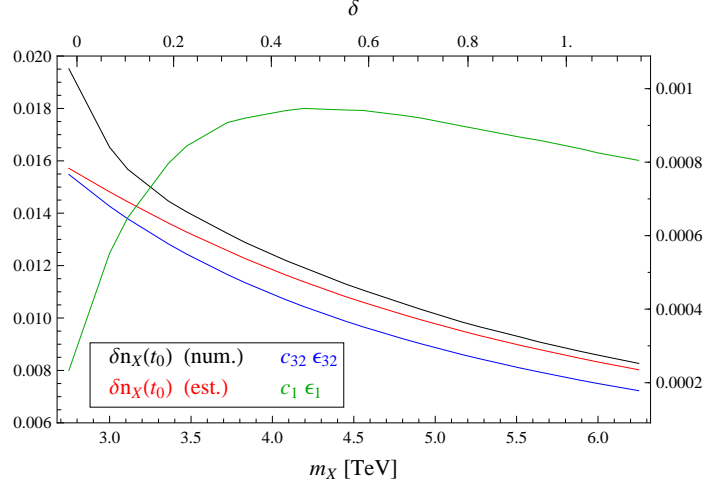


Figure 3: Fractional deviation of the relic abundance due to the SM electroweak phase transition, plotted against the WIMP mass and δ . The colors and axes are the same as in Figure 2

varying m_h and fixing $m_X = 6$ TeV, $g_X = 2$, and $\langle\sigma v\rangle = 2.33 \times 10^{-39} \text{ cm}^2$. As seen in the figure, the PT causes an $O(10^{-3} - 10^{-2})$ fractional increase in the relic abundance. We have chosen the DM mass to be 6 TeV such that freeze out and the PT coincide at $T \approx 303$ GeV for $m_h = 300$ GeV. For smaller m_h , the PT is delayed with respect to freezeout. The analytic estimate, given by Eq. (3.44), only receives contributions from the CC effect ($c_1\epsilon_1$ term) and the adiabatic decoupling effect ($c_{32}\epsilon_{32}$ term), because the PT is not first order. As we anticipated in the discussion of the preceeding paragraph, the ϵ_{32} term dominates. The analytic formula consistently underestimates the numerical calculation by 2–3%, and moreover, in the large m_h limit where $\delta \approx 0$, the deviation grows to approximately 4.5%. Both of these features can be traced back to approximations we have made in the analytic estimate. The first is associated with the approximation Eq. (B.5), which assumes the number density per comoving volume decreases significantly due to residual annihilations and introduces an $O(T_f/m_X) \lesssim 5\%$ error at all m_h . The second is associated with neglecting the equilibrium term n_X^{eq} in Eq. (3.2), which is not negligible at the start of the residual annihilation era. The scaling with m_h also has a simple, intuitive explanation. One can understand why $\delta n_X(t_0)$ is small at small m_h , because in this limit the PT occurs too late and becomes decoupled from freeze out. Considering the opposite limit, one may wonder if $\delta n_X(t_0)$ continues to increase for $m_h \gtrsim 300$ GeV where $\delta < 0$. For $\delta < 0$ the PT occurs before freeze out, as in the usual cosmology, and one would naively expect $\delta n_X(t_0) = 0$. Nevertheless, $\delta n_X(t_0)$ does continue to grow because of the way we have defined $n_X^{(U)}$. To calculate the usual relic abundance $n_X^{(U)}$ we

assume that there are 106.75 relativistic species at freeze out. If the PT occurs much earlier, the number of relativistic species at freeze out will be significantly less than 106.75 and $\delta n_X(t_0)$ will be non-zero. The CC contribution grows monotonically with decreasing m_h , since in this limit the PT temperature decreases and $c_1 \epsilon_1 \sim \rho_{\text{ex}}/T_{PT}^4$.

In Figure 3 we plot the relic abundance shift by fixing $m_h = 115$ GeV and varying m_X . At large m_X , freeze out occurs well before the PT, the two events decouple, and the relic abundance shift is small. At small $m_X \lesssim 2.8$ TeV, freeze out occurs after the PT, and the analytic estimate fails. The CC effect $c_1 \epsilon_1$ has a maximum of approximately 10^{-3} at $\delta_{max} \approx 0.5$. For $\delta > \delta_{max}$ the factor ϵ_1 , given by Eq. (3.20a), is small because T_f in the denominator is large. For $\delta < \delta_{max}$ the factor c_1 , given by Eq. (3.45a), is small because the CC is only present over a short time during WIMP residual annihilations. The presence of this maximum suggests that $c_1 \epsilon_1$ will typically be more sensitive to variations in the parameters of the scalar sector (e.g., m_h) than in variations of the DM sector (e.g., m_X). With this in mind, we will focus the remainder of our discussion on determining the conditions that a scalar potential must satisfy to maximize $c_1 \epsilon_1$.

We will now extend the estimates of Section 3 in order to understand Figure 2 through a simple analytic approximation. We focus on the CC contribution to $\delta n_X(t_0)$, given by Eq. (3.46), which is

$$\delta n_X(t_0) \ni c_1 \epsilon_1 \sim \frac{1}{10} \frac{\rho_{\text{ex}}}{g_E T_{PT}^4} \quad (4.1)$$

up to multiplication by an $O(1)$ function of δ . The factor of $g_E \approx 106.75$ represents the SM relativistic degrees of freedom before the PT. If we assume that before the PT, the SM particles are light with respect to the temperature, then we can approximate V_{eff} using the so-called high-temperature approximation

$$V_{\text{eff}}(h_c, T) \approx \frac{\lambda_{eff}}{4} (h_c^2 - v^2)^2 + c T^2 h_c^2. \quad (4.2)$$

Here we have defined

$$\lambda_{eff} \equiv \frac{4}{v^4} (V_{\text{eff}}(0, 0) - V_{\text{eff}}(v, 0)) \quad (4.3)$$

to be the one-loop effective self-coupling and $2cT^2$ is the thermal mass acquired by Higgs particles passing through the plasma. In the SM and subject to our renormalization scheme, these dimensionless numbers are $\lambda_{eff} \approx \lambda_{SM}$ and $c \approx c_{SM}$ where

$$c_{SM} = \frac{1}{24v^2} \left(6m_t^2 + 6m_b^2 + 6m_w^2 + 3m_z^2 + \frac{3}{2}m_h^2 \right) \approx 0.18 \quad (4.4a)$$

$$\lambda_{SM} = \frac{m_h^2}{2v^2} + \frac{1}{128\pi^2 v^4} (48m_t^4 + 48m_b^4 - 24m_w^4 - 12m_z^4 - (15 + \log 4)m_h^4) \approx 0.12 \quad (4.4b)$$

for $m_h \approx 115$ GeV. The PT occurs at a temperature T_{PT} where $\partial_{h_c}^2 V_{\text{eff}}(0, T_{PT}) = 0$. Solving for this temperature one obtains

$$c T_{PT}^2 = \frac{\lambda_{eff}}{2} v^2. \quad (4.5)$$

Before the PT, the CC energy density is

$$\rho_{\text{ex}} = V_{\text{eff}}(0, 0) = \frac{\lambda_{eff}}{4} v^4 \quad (4.6)$$

and we can estimate the deviation in the relic abundance using Eq. (4.1) to be

$$c_1 \epsilon_1 \sim \frac{1}{10} \frac{1}{g_E} \frac{c^2}{\lambda_{eff}}. \quad (4.7)$$

For natural couplings one expects $c^2/\lambda_{eff} \sim O(1)$ (e.g., $c_{SM}^2/\lambda_{SM} \approx 0.28$) and finds $c_1 \epsilon_1 \sim 1/(10g_E) \sim 10^{-3}$. Recalling also that $\lambda_{eff} \sim m_h^2$, one sees that this estimate agrees well with both the magnitude and scaling shown in Figure 2. Note that in the $\lambda_{eff} \rightarrow 0$ limit, we find that both ρ_{ex} and T_{PT} approach zero, but the ratio $\rho_{\text{ex}}/T_{PT}^4$ becomes large. This simple approximation suggests that the region of parameter space that maximizes the CC contribution to $\delta n_X(t_0)$ will have low temperature PTs. This is evident in Figure 2 because the CC effect grows at low m_h where the PT temperature is low. Hence we will next consider a model in which a scalar singlet coupled to the Higgs is introduced to lower the PT temperature.

4.2. SM Singlet Extension with \mathbb{Z}_2

In this section, we briefly discuss an extension of the Standard Model in which the presence of an additional scalar field modifies the electroweak PT dynamics. However, we show that the dark matter relic abundance is not significantly enhanced, and we argue that we should consider models with first order PTs. Consider an extension of the SM in which a real, singlet, scalar field $s(x)$ is coupled to the Higgs $h(x)$ through interactions which respect the \mathbb{Z}_2 symmetry $s \rightarrow -s$. The renormalized potential for this theory can be written as

$$U(\{h, s\}) = \frac{m_h^2}{8v^2} (h^2 - v^2)^2 + \frac{b_4}{4} s^4 + \frac{1}{2} m_s^2 s^2 + \frac{a_2}{2} s^2 (h^2 - v^2) \quad (4.8)$$

such that $\partial_h U(\{v, 0\}) = 0$, $\partial_h^2 U(\{v, 0\}) = m_h^2$ and $\partial_s^2 U(\{v, 0\}) = m_s^2$. We require

$$m_s^2 - a_2 v^2 > 0 \quad \text{and} \quad 2a_2 + b_4 + \frac{m_h^2}{2v^2} > 0 \quad (4.9)$$

to ensure $\langle s \rangle = 0$. This model, known as the \mathbb{Z}_2 xSM, has been previously studied in order to determine the viability of s as a dark matter candidate [53–58]. We will not restrict ourselves to this scenario, but instead treat the dark matter as a separate sector. The role of s is simply to modify the PT dynamics.

Since this model possesses a greater parametric freedom than the SM, we can attempt to verify the relationship Eq. (4.7), derived in the previous section, which relates $c_1\epsilon_1 \sim c^2/\lambda_{eff}$. This is accomplished by first mapping the parameters of the \mathbb{Z}_2 xSM to c and λ_{eff} , and second by performing a parameter scan while calculating $c_1\epsilon_1$. We obtain c and λ_{eff} by calculating the thermal effective potential as described in the previous section (see also Appendix F). If we assume that the quanta of $s(x)$ are light with respect to the temperature, we can then extract c and λ_{eff} by matching the effective potential to Eq. (4.2). Doing so yields the expressions

$$c = c_{SM} + \frac{a_2}{24} \quad (4.10)$$

$$\lambda_{eff} = \lambda_{SM} - \frac{a_2^2}{32\pi^2} \psi\left(\frac{a_2 v^2}{m_s^2}\right) \quad (4.11)$$

$$\psi(x) \equiv 3 - \frac{2}{x} - 2\left(1 - \frac{2}{x} + \frac{1}{x^2}\right) \log[1 - x] \quad (4.12)$$

where the terms containing a_2 arise from 1-loop diagrams with an s -particle in the loop, and the function ψ varies from $\psi(0) = 0$ to $\psi(1) = 1$. As a result of the minus sign in Eq. (4.11), there is an upper bound $a_2 \lesssim 5$ given by the constraint $\lambda_{eff} > 0$. Now we can see the impact of the singlet field on the PT. For $a_2 > 0$, the parameter c is slightly larger and λ_{eff} is slightly smaller than in the SM. Recall that the PT temperature, given by Eq. (4.5), scales like $T_{PT}^2 \sim \lambda_{eff}/c$. Hence, the singlet field lowers the PT temperature and makes the CC energy density relatively more significant, which causes the relic abundance shift to be greater.

To verify these analytic arguments, we calculate the PT temperature and $c_1\epsilon_1$ numerically over a region of the theory space. We allow m_h^2 and a_2 to vary in the ranges $m_h^2 \in [(50 \text{ GeV})^2, (300 \text{ GeV})^2]$ and $a_2 \in [-0.1, 4.0]$, and we fix $b_4 = 0.25$ and $m_s^2 = (500 \text{ GeV})^2$. The range for m_h is chosen to prevent the Higgs from becoming unacceptably light⁷, while the range for a_2 is chosen to satisfy Eq. (4.9) and to avoid the unitarity bound. We map m_h^2 and a_2 to c and λ_{eff} using Eqs. (4.10) and (4.11). In Figure 4, we have plotted the contribution to $\delta n_X(t_0)$ from the CC effect ($c_1\epsilon_1$) over the $c^2/\lambda_{eff}-m_h$ plane. This figure shows that the CC effect grows with increasing c^2/λ_{eff} and

⁷ Mixing with the singlet does not significantly reduce the LEP Higgs search bound [54]. Moreover, for small m_h the electroweak breaking minimum may become metastable [53, 59], and the PT becomes first order [60]. Nevertheless, we have allowed m_h to be as small as 50 GeV to illustrate the parametric dependence of the CC effect.

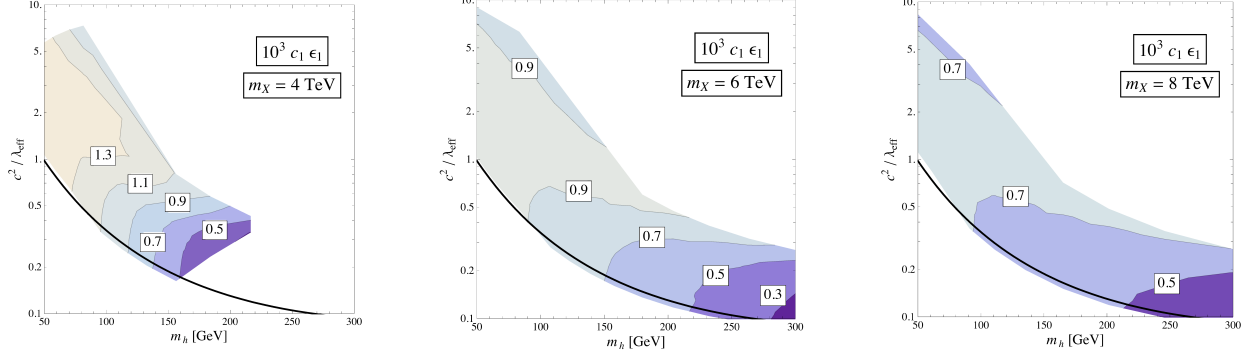


Figure 4: The CC contribution to $\delta n_X(t_0)$, given by the $c_1 \epsilon_1$ term of Eq. (3.44), plotted over the $c^2 / \lambda_{eff} - m_h$ plane for three values of m_X . The black line represents the SM ($a_2 = 0$).

decreasing m_h , as we anticipated in Eq. (4.7). The largest value of $c_1 \epsilon_1$ is approximately 1.3×10^{-3} , which is only about 40% larger than in the SM. The insignificant enhancement can be understood by observing that although $a_2 > 0$ tends to decrease c , given by Eq. (4.10), its contribution is suppressed by a factor of 24. Since $c_{SM} \approx 0.18$ we run into the unitarity bound on a_2 before it contributes significantly to c . If we were to add N light singlet fields instead of one, the contribution to c would be $N a_2 / 24$, which can be order one even for small a_2 . We have not take this approach here because the N additional relativistic degrees of freedom would have a larger effect on the relic abundance by increasing the energy density of radiation than through the CC. We have also plotted $c_1 \epsilon_1$ for three different values of the WIMP mass from 4 to 8 TeV. This narrow range of viable parameters illustrates the tuning that is required to ensure that the PT and freeze out occur at the same time. If the WIMP mass is too large, freeze out occurs too long before the PT when the CC energy density was subdominant to the energy density of the plasma. As the WIMP mass is lowered, the delay between freeze out and the PT decreases and $c_1 \epsilon_1$ grows. If the WIMP mass is too small, freeze out occurs after the PT when the CC energy density has been converted into radiation. This is the case in the $m_h \gtrsim 200$ region of the $m_X = 4$ TeV plot.

The examples of the SM and the \mathbb{Z}_2 xSM demonstrate that it is challenging to obtain $c_1 \epsilon_1$ larger than $O(10^{-3})$. Our discussion at the end of Section 4.1 and simple dimensional analysis illustrate why this is the case. In that calculation we obtained Eq. (4.7) which can be written schematically as $c_1 \epsilon_1 \sim \rho_{ex} / T_{PT}^4 \sim c^2 / \lambda_{eff}$. Note that the mass scale v , which controls both ρ_{ex} and T_{PT} , cancels out in the ratio ρ_{ex} / T_{PT}^4 . In light of Eq. (4.7) we propose that the CC effect can be enhanced by working in a model that has multiple mass scales if there exists a hierarchy between them. We will

explore different applications in the remainder of this section.

4.3. Generic Single Scalar Model

In this section we calculate the CC contribution to the relic abundance shift in a generic single scalar model. Although extensions of the Standard Model typically contain multiple scalar degrees of freedom related by symmetries, the thermal dynamics (supercooling and reheating) of a symmetry breaking PT can often be modeled by a single scalar degree of freedom which does not display the symmetries of the full theory [9, 61]. With this motivation in mind, we consider the theory of a real scalar field $\varphi(x)$ coupled to N Dirac fields $\psi_i(x)$. The scalar field will experience a first order PT during which dark matter freezes out, and the light fermions will compose the hot thermal bath. Using this construction, we will be able to calculate the CC effect, which is related to the non-thermal energy density and the amount of supercooling, but we cannot estimate the entropy and decoupling effects since these depends on how φ is coupled to the full theory. Therefore, in this section we assume no decoupling occurs near the time of the PT and that the number of relativistic species is fixed to $g_{E/S} \approx 106.75$, the relativistic SM background. Let the action be given by

$$S[\varphi] = \int d^4x \left\{ \frac{1}{2}(\partial\varphi)^2 - U(\varphi) - \sum_{i=1}^N \bar{\psi}_i (i\not{\partial} - m_i - h_i\varphi) \psi_i + \mathcal{L}_{\text{ct}} \right\} \quad (4.13)$$

where

$$U(\varphi) = \rho_{\text{ex}} + \frac{1}{2}M^2\varphi^2 - \mathcal{E}\varphi^3 + \frac{\lambda}{4}\varphi^4 \quad (4.14)$$

is the renormalized potential and \mathcal{L}_{ct} is the counterterm Lagrangian. Note that we have eliminated the tadpole term in $U(\varphi)$ by defining the origin in field space appropriately, but there is still a counterterm for the tadpole in \mathcal{L}_{ct} . As discussed in Section 4.2, we expect that there will be a greater impact on the dark matter relic abundance if freeze out occurs during a first order PT with large supercooling. Hence, we would like to understand what region of parameter space yields a PT of this kind. In particular, we expect that large supercooling can be obtained if the theory $S[\varphi]$ possesses two vacua, which will correspond to the low- and high-temperature phases, and that the vacua are separated by a barrier.

We can determine the vacuum structure by identifying the minima of the effective potential, which is calculated in Appendix F. Provided that the non-thermal radiative corrections are negligible, the effective potential can be approximated as $V_{\text{eff}}(\varphi_c, T=0) \approx U(\varphi_c)$. It is convenient to

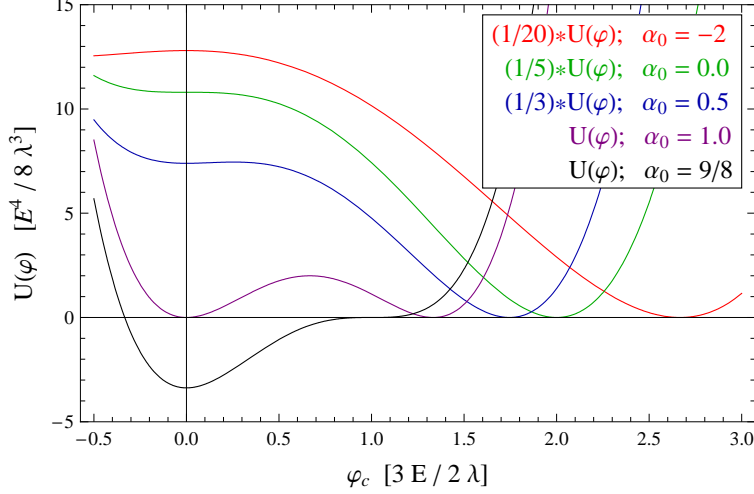


Figure 5: An illustration of the α_0 dependance of the potential given by Eq. (4.14). The curves represent $\alpha_0 = -2$ (red), $\alpha_0 = 0$ (green), $\alpha_0 = 0.5$ (blue), $\alpha_0 = 1$ (purple), and $\alpha_0 = 9/8$ (black).

eliminate M^2 for the dimensionless quantity $\alpha_0 \equiv \lambda M^2 / 2\mathcal{E}^2$ while assuming $\lambda\mathcal{E} \neq 0$. We now see that the parameter α_0 controls the shape of the potential $U(\varphi)$: for $\alpha_0 = 1$, the potential has two degenerate minima at $\varphi_c = 0$ and $\varphi_c = v|_{\alpha_0=1}$ where

$$v = \frac{3\mathcal{E}}{2\lambda} \left(1 + \sqrt{1 - \frac{8}{9}\alpha_0} \right); \quad (4.15)$$

for $\alpha_0 > 1$, $\varphi_c = 0$ is the global minimum; for $0 < \alpha_0 < 1$, $\varphi_c = v$ is the global minimum; and for $\alpha_0 < 0$, $\varphi_c = 0$ becomes a maximum (see also Figure 5). Therefore, provided that we take $0 \lesssim \alpha_0 \lesssim 1$, the theory possesses a metastable vacuum in which $\varphi_c \approx 0$ and a stable vacuum in which $\varphi_c \approx v$. In the stable vacuum, we impose the tuning condition $V_{\text{eff}}(v, 0) = 0$ to solve for

$$\rho_{\text{ex}} \approx \frac{\mathcal{E}^4}{8\lambda^3} \left[27 - 36\alpha_0 + 8\alpha_0^2 + 27 \left(1 - \frac{8}{9}\alpha_0 \right)^{3/2} \right] + O(\hbar), \quad (4.16)$$

which represents the CC energy density prior to the PT. Finally, the barrier separating the two vacua has a “height”

$$V_{\text{barrier}} = U(\text{barrier}) - U(0) \approx \frac{4\mathcal{E}^4\alpha_0^3}{27\lambda^3} \left[1 + O(\alpha_0) \right] \quad (4.17)$$

relative to the metastable vacuum. Due to the factor of α_0^3 , the barrier vanishes rapidly as α_0 approaches zero. This is illustrated by the $\alpha_0 = 0.5$ curve of Figure 5 in which the barrier is already almost imperceptible to the eye.

Having established that this theory admits two vacua, we will study the PT using the thermal effective potential. Although the numerical calculations use the full effective potential, we can gain some intuition by making the high temperature approximation. We assume that the ψ_i -particles are light with respect to the temperature of the thermal bath, $m_i^2 \ll T^2$, and that the φ -particles are heavy. In this limit, then the one-loop thermal effective potential may be approximated by the high temperature expansion

$$V_{\text{eff}}(\varphi_c, T) \approx U(\varphi_c) + cT^2\varphi_c^2 + O(m_i^2/T^2) + O(\hbar) \quad (4.18)$$

where $c \approx \sum_{i=1}^N h_i^2/12$ is related to the couplings between φ and ψ_i . Just as we introduced α_0 to reparametrize $V_{\text{eff}}(\varphi_c, 0)$, we can now introduce

$$\alpha(T) = \alpha_0 \left(1 + \frac{\lambda c}{\mathcal{E}^2 \alpha_0} T^2 \right) \geq \alpha_0 \quad (4.19)$$

to parameterize $V_{\text{eff}}(\varphi_c, T)$. This definition is particularly convenient, because now Figure 5 also illustrates the temperature dependence of $V_{\text{eff}}(\varphi_c, T)$ (up to φ_c -independent terms) if one replaces α_0 with $\alpha(T)$. We obtain the expectation values of φ in the “symmetric” and “broken” phases, $v^{(s)}(T)$ and $v^{(b)}(T)$, by solving $(\partial/\partial\varphi_c)V_{\text{eff}}(\varphi_c, T) = 0$ subject to the boundary conditions $v^{(b)}(0) = v$ and $v^{(s)}(0) = 0$. We use the terms “symmetric” and “broken,” even though $S[\varphi]$ does not display a symmetry in order to connect with the notation of Section 2.

Provided that this model experiences a first order PT, the CC’s effect on the relic abundance will depend sensitively on the amount of supercooling at the PT. This is seen by the factor of $(T_f)^4 \approx (T_{PT}^-)^4$ in Eq. (3.20a). Therefore, we will begin by investigating the parametric dependence of the amount of supercooling, and we will see that it has an interesting dependence on the parameter α_0 . The supercooling stage begins when the temperature drops below

$$T_c \approx \mathcal{E} \sqrt{\frac{1 - \alpha_0}{\lambda c}}, \quad (4.20)$$

defined by Eq. (2.2), or equivalently when $\alpha(T_c) = 1$. During supercooling, the universe remains in the metastable, symmetric phase until bubbles of the broken phase begin to nucleate. Bubble nucleation is a non-perturbative process [62], and it occurs at a rate per unit volume which carries the standard exponential suppression $\Gamma \sim T^4 \exp[-S^{(3)}/T]$, where $S^{(3)}(T)$ is the action of the O(3) symmetric bounce [63–65]. Provided that $V_{\text{eff}}(\varphi_c, T)$ can be expressed in the form of Eq. (4.18),

then $S^{(3)}$ is well approximated by the empirical formula [66]

$$\frac{S^{(3)}}{T} \approx 13.7 \frac{\mathcal{E}}{T} \left(\frac{\alpha}{\lambda} \right)^{3/2} f(\alpha) \quad (4.21)$$

$$f(\alpha) \equiv 1 + \frac{\alpha}{4} \left(1 + \frac{2.4}{1-\alpha} + \frac{0.26}{(1-\alpha)^2} \right) \quad (4.22)$$

with $\alpha = \alpha(T)$. Bubbles form rapidly once the bubble nucleation rate averaged over a Hubble volume ΓH^{-3} is comparable to the Hubble expansion rate $H \sim T^2/M_p$. For an electroweak scale PT, this equality occurs when $S^{(3)}/T$ drops below approximately 140 [67, 68]. Therefore, we can determine the amount of supercooling by solving $S^{(3)}/T \approx 140$ for $T = T_{PT}^-$ and comparing this temperature with T_c .

Considerations of the equation $S^{(3)}/T \approx 140$ demonstrate that the nature of the PT is strongly dependent upon the vacuum structure of the theory, as parametrized by α_0 . We will discuss the two cases $\alpha_0 > 0$ and $\alpha_0 < 0$ separately. For $\alpha_0 > 0$, the vacuum with $\varphi_c = 0$ remains metastable as $T \rightarrow 0$. This implies that T_{PT}^- can be arbitrarily low, and in this limit of large supercooling the CC effect may be arbitrarily large. However, in this case the barrier in $V_{\text{eff}}(\varphi_c, T)$ persists as $T \rightarrow 0$, and it is possible that the PT does not occur at any temperature, but instead that the universe becomes trapped in the metastable vacuum. This follows from the observation that for $\alpha_0 > 0$, $S^{(3)}/T$ has a minimum at finite T : at low temperatures $S^{(3)}/T$ grows due to the explicit factor of T in the denominator, and at high temperatures $f(\alpha)$ diverges as T approaches T_c and $\alpha \rightarrow 1$. For $\alpha_0 \lesssim 1$ the inequality $S^{(3)}/T \lesssim 140$ is not satisfied at any temperature, and the PT does not occur⁸. Therefore, if we require that the PT must occur via thermal bubble nucleation, we obtain an upper bound on α_0 . On the other hand, for the case $\alpha_0 < 0$, the PT necessarily occurs at a temperature $T_{PT}^- > 0$, since the symmetric phase becomes perturbatively unstable at low temperatures. This latter case has the drawback that supercooling cannot last an arbitrarily long time.

Assuming that the PT does occur, we can quantify the amount of supercooling using

$$\delta_{SC} = 1 - \frac{T_{PT}^-}{T_c}, \quad (4.23)$$

which takes values between 0 and 1. Parametrizing the temperature dependence with δ_{SC} , we can

⁸ At least, the PT does not occur as a thermal process, although it may still occur as a quantum tunneling process [64]. However, since quantum tunneling typically proceeds on a longer time scale, the universe could enter an inflationary phase, which leads to a cosmological history that deviates significantly from the perturbations we consider in Section 3.

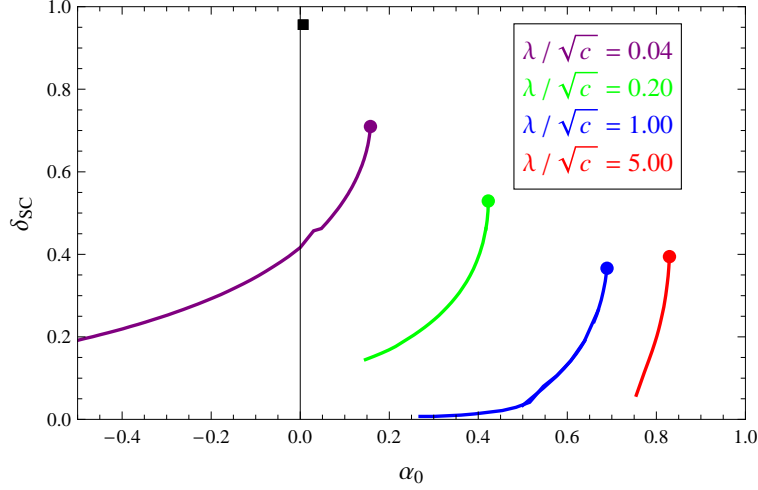


Figure 6: The amount by which the PT temperature drops below the critical temperature, quantified by δ_{SC} , is plotted against the parameter α_0 which controls the height of the barrier. The curves represent $\lambda/\sqrt{c} = 0.04$ (purple), 0.20 (green), 1.00 (blue), and 5.00 (red). The square indicates the especially tuned parameter set given by Eq. (4.28).

rewrite Eq. (4.21) as

$$\frac{S^{(3)}}{T} \Big|_{T_{PT}^-} \approx 13.7 \left(\frac{\lambda}{\sqrt{c}} \right)^{-1} \frac{\alpha^{3/2}}{\sqrt{1-\alpha_0}} \frac{f(\alpha)}{1-\delta_{SC}} \quad (4.24)$$

$$\alpha = \alpha_0 + (1-\alpha_0)(1-\delta_{SC})^2, \quad (4.25)$$

which is now only a function of α_0 , λ/\sqrt{c} , and δ_{SC} . Of course, this expression is approximate, since we assumed V_{eff} took the form of Eq. (4.18), but it suggests that the amount of supercooling will depend most sensitively on α_0 and λ/\sqrt{c} . Now using the full thermal effective potential, we impose $S^{(3)}/T|_{T_{PT}^-} = 140$ and solve for δ_{SC} , which we have plotted in Figure 6 for various parameter sets:

$$\begin{aligned} \mathcal{E} &= 5 \text{ GeV} & \lambda &= \{0.004, 0.02, 0.10, 0.50\} \\ N &= 1 & m &= 10 \text{ GeV} & h &= 0.346 & c &\approx 0.01. \end{aligned} \quad (4.26)$$

The supercooling grows with increasing α_0 and decreasing λ/\sqrt{c} as the barrier height and bounce action are made larger. The amount of supercooling is typically $\delta_{SC} = O(0.5)$ which implies $T_{PT}^- = O(T_c/2)$. Above a finite value of α_0 (indicated by a dot) the barrier becomes insurmountably large, and the universe becomes trapped in the metastable vacuum. The largest amount of supercooling is achieved for $\lambda/\sqrt{c} \ll 1$ and $0 < \alpha_0 \ll 1$. In this parameter regime the CC is large (see Eq. (4.16)), and the metastable vacuum is separated from the true vacuum by small barrier (see Eq. (4.17)).

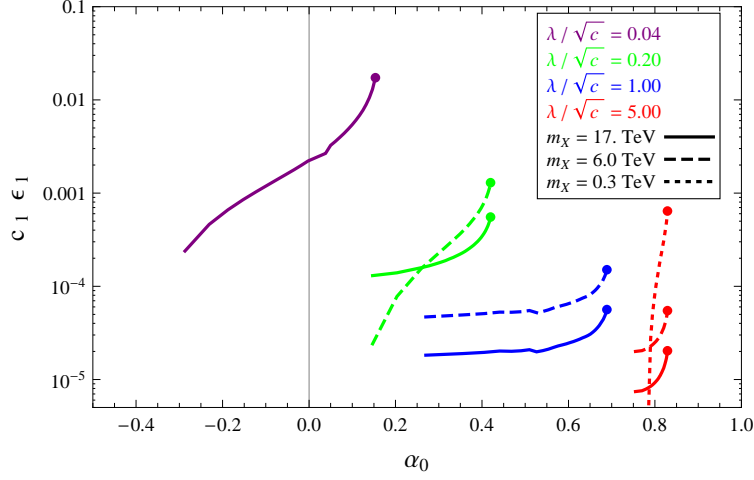


Figure 7: The CC effect on the relic abundance $c_1\epsilon_1$ plotted against α_0 for $m_X = 17$ TeV (solid), 6 TeV (dashed), and 0.3 TeV (dotted). For the contours which are absent, freeze out occurs after the PT when the CC is not EW-scale.

Having come to understand the parametric dependance of the amount of supercooling as φ experiences a first order PT, we turn our attention back to calculating the impact of such a PT on dark matter freeze out. Using Eq. (3.46) we calculate the effect of the CC on the relic abundance shift and present the results in Figure 7. We have chosen the same parameters as indicated in Eq. (4.26) and have taken

$$m_X = \{0.3, 6.0, 17\} \text{ TeV} \quad g_X = 2 \quad \langle\sigma v\rangle = 2.33 \times 10^{-39} \text{ cm}^{-2} \quad (4.27)$$

as well. The figure illustrates that is possible to achieve $c_1\epsilon_1 = O(0.01)$ in the tuned parametric regime where λ/\sqrt{c} is small and α_0 approaches its maximally allowed value. Some of the curves are absent for the smaller WIMP masses. This occurs because as m_X is lowered, the temperature of freeze out decreases as well. In the case that λ/\sqrt{c} is small and the PT temperature is high (see Eq. (4.20)), freeze out will occur after the PT for small m_X . This statement about the relative times of freeze out and the PT also explains why $c_1\epsilon_1$ is insensitive to α_0 for certain parameter sets (e.g., $\lambda/\sqrt{c} = 1$, $m_X = 17$ TeV) and very sensitive for others (e.g., $\lambda/\sqrt{c} = 5$, $m_X = 0.3$ TeV). In the first case, freeze out occurs long before the PT while in the latter case, freeze out occurs just before and during the PT and there is a large impact on the relic abundance.

To conclude this section, we present a particular tuned parameter set which yields $c_1\epsilon_1 = O(1)$.

Suppose that we have only one fermion ψ and the parameters of $S[\varphi]$ are given by

$$\begin{aligned} \lambda &= 5.4 \times 10^{-4} & h &= 0.1 \\ \mathcal{E} &= 0.27 \text{ GeV} & M^2 &= (1.89 \text{ GeV})^2 & m &= 10 \text{ GeV} \end{aligned} \quad (4.28)$$

which leads to

$$\begin{aligned} v &\approx 1497 \text{ GeV} & \alpha_0 &\approx 0.007 \\ c &\approx 8.3 \times 10^{-4} & \frac{\lambda}{\sqrt{c}} &\approx 0.018 \end{aligned} \quad (4.29)$$

and PT temperatures

$$T_c \approx 374 \text{ GeV} \quad T_{PT}^- \approx 16 \text{ GeV} \quad \delta_{SC} \approx 0.96. \quad (4.30)$$

This parameter set is represented on Figure 6 by a square marker. In the dark matter sector we take

$$m_X = 600 \text{ GeV} \quad g_X = 2 \quad \langle \sigma v \rangle = 2.33 \times 10^{-39} \text{ cm}^{-2} \quad (4.31)$$

such that

$$T_f \approx 34 \text{ GeV} \quad \text{and} \quad \delta \approx 1.12. \quad (4.32)$$

Using these values we can estimate the CC effect as

$$c_1 \epsilon_1 \approx 6.1 \quad (4.33)$$

Note that the potential obtained with these parameters has a very shallow metastable vacuum at $\varphi_c \approx 0$, separated from the global vacuum at $\varphi_c \approx v$ by a very small barrier.

4.4. Singlet Extension with First Order PT

In this section, we consider a generalization of the SM extension studied in Section 4.2, in which we do not impose a \mathbb{Z}_2 symmetry on the singlet field $s(x)$. This leads to model known as the xSM [53, 54]. The xSM admits a first order electroweak PT [61, 69], and we seek to compute the effect on the relic abundance due to the effective CC at the PT. As discussed in Section 4.3, the CC effect grows with the duration of supercooling. With this in mind, we will focus on a region of parameter space in which we expect to have first order PTs with large supercooling. Supercooling

is an example of the hierarchy of mass scales which we argued in Section 4.2 helps to obtain a larger CC effect.

We generalize the \mathbb{Z}_2 xSM potential Eq. (4.8) by relaxing the \mathbb{Z}_2 symmetry. This allows us to write down the three additional operators sh^2 , s^3 , and s , but we eliminate the tadpole by an appropriate shift in the field space. We are left with the xSM renormalized potential

$$U(\{h, s\}) = \frac{m_h^2}{8v^2} (h^2 - v^2)^2 + \frac{b_4}{4} s^4 + \frac{1}{2} m_s^2 s^2 + \frac{b_3}{3} s^3 + \frac{1}{2} s (h^2 - v^2) (a_1 + a_2 s). \quad (4.34)$$

The thermal effective potential V_{eff} is calculated in Appendix F. With this parametrization, $V_{\text{eff}}(\{h_c, s_c\}, T = 0)$ has a minimum at $\{h_c, s_c\} = \{v, 0\}$ where $V_{\text{eff}}(\{v, 0\}, T = 0) = 0$ and the curvatures in the h and s directions are m_h^2 and m_s^2 respectively. The Higgs vacuum expectation value is fixed by electroweak constraints, but the six real numbers $\{m_h^2, m_s^2, b_4, b_3, a_1, a_2\}$ are free parameters.

As in the previous section, we compute the bounce action $S^{(3)}$ in order to estimate the PT temperature T_{PT}^- by solving $S^{(3)}/T \approx 140$. This calculation is made more challenging by the presence of the additional field direction. To obtain $S^{(3)}$ we make the approximation that the PT occurs along the trajectory $\bar{s}(h_c)$ satisfying

$$\left. \frac{dU(\{h_c, s_c\}, 0)}{ds} \right|_{\bar{s}_c} = 0 \quad \text{and} \quad \bar{s}_c(v) = 0, \quad (4.35)$$

which reduces the problem back to solving for the bounce in one dimension. In the region of parameter space on which we are focused, this approximation gives T_{PT}^- to within a few percent (see Appendix G for details). Note that the empirical formula Eq. (4.21) cannot be applied here, because the effective potential is not well approximated by the form Eq. (4.18).

We have performed a parameter space scan and searched for a region with large corrections to the relic abundance from the CC. In the scan we fix the parameters $b_3 = -20$ GeV, $b_4 = 0.2$, $a_1 = -25$ GeV, and $a_2 = 0.2$, and we vary $m_h^2 \in [(65 \text{ GeV})^2, (170 \text{ GeV})^2]$ and $m_s^2 \in [(40 \text{ GeV})^2, (140 \text{ GeV})^2]$. In order to connect with the intuition garnered from the single field model of Section 4.3, we have mapped the xSM parameter space to a single parameter M^2 . This is accomplished by restricting to the trajectory given by Eq. (4.35) and defining

$$M^2 \equiv \left. \frac{d}{dx^2} V_{\text{eff}}(\{h_c(x), \bar{s}_c(h_c(x))\}, T = 0) \right|_{x=0} \quad (4.36)$$

where x parametrizes the position along the curve $\bar{s}_c(h)$. The parameter M^2 controls the stability of the electroweak preserving vacuum: if $M^2 > 0$ the symmetric phase remains metastable as $T \rightarrow 0$,

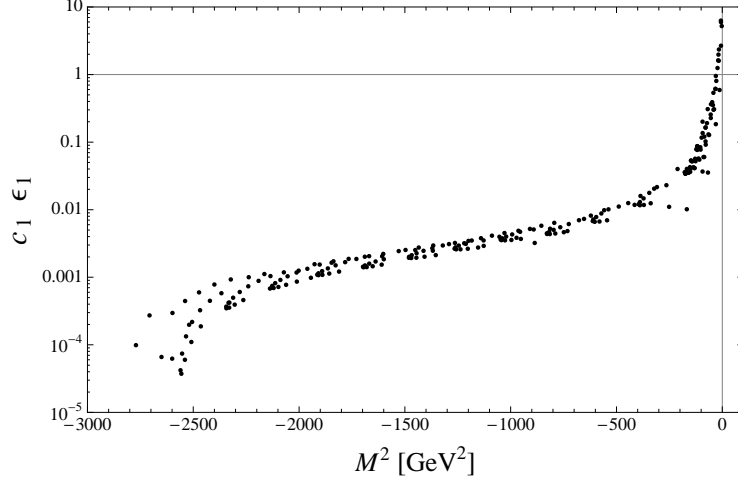


Figure 8: The fractional deviation in the relic abundance of a 2 TeV WIMP due to the CC at the xSM electroweak PT. The parameter M^2 controls the curvature of the zero temperature effective potential along the PT trajectory. For $M^2 \lesssim 0$ large supercooling enhances the CC's effect. For $M^2 \gtrsim 0$ the PT does not occur, and for $M^2 \lesssim -2500 \text{ GeV}^2$ the PT occurs before freeze out leading to a suppression of the relic abundance shift.

whereas if $M^2 < 0$ the symmetric phase becomes perturbatively unstable at some finite temperature $T_0 > 0$. In this way, the potential depends on the parameter M^2 in the same way as the parameter α_0 from Section 4.3. We cannot map the xSM parameter space to α_0 directly because the effective potential along the trajectory Eq. (4.35) cannot be expressed in the form of Eq. (4.18).

In Figure 8, we have plotted $c_1\epsilon_1$, given by Eq. (3.46), by projecting onto the M^2 axis and choosing $m_X = 2 \text{ TeV}$. For $M^2 \lesssim 0$ the CC has an $O(1)$ impact on the relic abundance. In this region, the supercooling is maximal and $T_{PT}^- \gtrsim T_0 = O(\text{few GeV})$. For smaller values of M^2 , the CC effect rapidly decreases and drops below 1% for $M^2 \lesssim 500 \text{ GeV}^2$. Therefore, in order for the CC to have a significant impact on the relic abundance, the parameters of the scalar sector must be tuned into a narrow band where supercooling is large. In Figure 9, we have allowed the WIMP mass to decrease to 500 GeV. This change lowers the freeze out temperature, reduces the delay δ between freeze out and the PT, and therefore increases the CC effect. However, this increase is small compared with the amount by which $c_1\epsilon_1$ varies with M^2 in the $M^2 \lesssim 0$ region. For smaller values of M^2 , the PT temperature is higher and for the 500 GeV WIMP, freeze out occurs after the PT causing the CC effect to be suppressed. These calculations lead us to the conclusion that the optimal region of parameter space is one in which the symmetric phase becomes perturbatively unstable at a low temperature and the effective potential is concave at zero temperature. We were

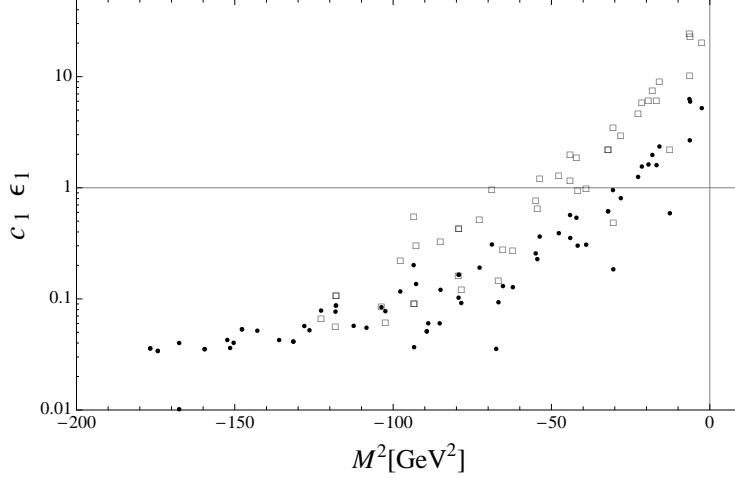


Figure 9: This figure shows a subset of Figure 8 as well as the CC effect for a 500 GeV WIMP represented by squares. As the WIMP mass is reduced, freeze out occurs at a lower temperature. This increases $c_1\epsilon_1$ for $M^2 \lesssim 0$ where the PT temperature is low, but excludes points $M^2 \lesssim -100 \text{ GeV}^2$ where freeze out occurs after the PT.

unable to find any points with $M^2 > 0$ in which the PT completes.

The following is a benchmark parameter point:

$$\begin{aligned}
 \{a_1, b_3, m_h, m_s, m_X\} &= \{-25, -20, 128, 91.1, 2000\} \text{ GeV}, & \{a_2, b_4\} &= \{0.2, 0.2\}, \\
 M^2 = -47.7 \text{ GeV}^2 & \quad \{T_f, T_c, T_{PT}^+, T_{PT}^-, T_0\} = \{107, 70.7, 30.0, 13.7, 12.7\} \text{ GeV}, \\
 c_1\epsilon_1 &= 0.390, & \rho_{\text{ex}} &= (69.7 \text{ GeV})^4.
 \end{aligned} \tag{4.37}$$

The scalar masses are given by the eigenvalues of Eq. (F.16) which are

$$\begin{aligned}
 M_H &= 141 \text{ GeV} & \{0.78, 0.22\} \\
 M_S &= 70.7 \text{ GeV} & \{0.22, 0.78\}
 \end{aligned} \tag{4.38}$$

with the respective squared eigenvectors indicated to the right.

5. CONCLUSION

We have considered a way to probe the hypothesis that the present-day, minute CC energy density is the result of a tuning between UV contributions of unspecified origin and IR contributions that arise from cosmological PTs. Prior to the electroweak scale PT, the UV contribution would have been partially uncanceled leaving an $O(M_W^4)$ energy density. It is possible to probe this energy

density with the physics of dark matter freeze out provided that the dark matter mass is greater than a few hundred GeV. The dark matter relic abundance is increased due to the effective CC's contribution to the Hubble expansion rate during freeze out.

The notion of how an effective vacuum energy (which is Lorentz invariant in the flat space limit) can depend on temperature (which manifestly breaks Lorentz invariance) has been clarified. The temperature is an approximation to the mixed vacua, inhomogeneous states whose occupation is very probable near the time of the PT. This leads to a spatially averaged equation of state that is expressed in terms of an effective vacuum energy density that is somewhere between the false and true vacuum energy densities. The true inhomogeneous field configurations may also lead to additional dark matter freeze out effects that have not been investigated in this paper. This would be an interesting avenue for future investigations.

To provide a generic prediction associated with the established physics and to provide the computational details missing in [9], we have analyzed the Standard Model with a 115 GeV Higgs and a single WIMP dark matter degree of freedom, assuming that the WIMP interaction effects on the dynamics of the PT is negligible. We have found that the CC causes an $O(10^{-3})$ fractional increase in the relic abundance of a 4 TeV WIMPs. This is typical of non-first order PTs.

We have also investigated minimal singlet extensions of the SM and searched for parametric regimes in which the CC effect on the relic abundance is enhanced. We find that a low temperature, first order PT with large supercooling is the optimal scenario for maximizing the CC effect. In this limit, the effective CC energy density's contribution to the Hubble expansion rate can be comparable to the radiation energy density, and the CC effect can become order one. In the context of a generic single field model, we find that reaching this limit requires a tuning of the scalar sector parameters and the WIMP mass. Without appropriate tuning, either 1) the PT will not occur at all by thermal bubble nucleation, 2) the PT will occur before freeze out (when the dark matter is still in equilibrium and the CC effect is suppressed), or 3) the CC effect will not be large.

As a specific example, we have considered the xSM, an extension of the SM that adds a real scalar singlet. In that model, we find that the CC may increase the relic abundance by as much as a factor of order few. To maximize the CC effect, the scalar parameters must be tuned into a narrow band where fluctuations around the symmetric “vacuum” are slightly tachyonic, which allow for a long period of supercooling. The magnitude of the CC effect is relatively insensitive to the WIMP mass provided that the latter is sufficiently large such that freeze out begins before the PT occurs.

The tests of CC fine tuning hypothesis are notoriously rare. In the context of a dark matter

probe, it is encouraging that parametric possibilities do exist within simple extensions of the SM. It would be interesting to further advance this exploration by computing the dark matter implications of modified gravity/self-tuning models and comparing the results with those of this paper. Furthermore, it would be interesting to cross correlate other astrophysical tests of those modified gravity/self-tuning models with the dark matter predictions made within those models. Note also that there are other probes of the cosmological constant during a PT such as gravity wave probes [70] that will need more development as the gravity wave spectrum calculational technology improves [71–73].

Appendix A: Renormalization Scale

Any measurable quantity is independent of the renormalization scale. Hence, one should not expect that the running of the cosmological constant parameter should affect any physical observable. Indeed, the running of the other parameters in the Lagrangian will compensate the running of the CC parameter to yield the same T_{00} governing the expansion rate H which can be measured for example by a test photon redshift. The renormalization scheme and scale does however determine the manner in which radiative corrections play a role. Furthermore, in any practical computations involving finite order truncation in \hbar expansion, there is a renormalization scale dependence to next order in the perturbation power unless one is able to explicitly keep exactly the terms of the relevant order in \hbar .

Given that we are computing homogeneous quantities, one might also naively worry that there is a coarse graining requirement down to length scales of H^{-1} . To see why this is not the case and to see what renormalization scales would minimize the radiative correction dependence, consider the effective action generating the gravitational equation of motion for the metric g :

$$e^{iS_{\text{eff}}[g]} = e^{iS_{EH}[g]} \int D_\Lambda \phi e^{iS_M[g,\phi]} \quad (\text{A.1})$$

where S_{EH} is the Einstein-Hilbert action, the matter field schematically written as ϕ satisfies the appropriate boundary conditions relevant for the matter distribution, and we assume a renormalization scale at Λ . Since we are going to resolve the one-particle thermal states with masses of order the freeze out temperature T_f , we should have $\Lambda \gtrsim T_f$. Semiclassically expanding about the classical path ϕ_0 on the right hand side of Eq. (A.1), we have

$$e^{iS_{\text{eff}}[g]} = e^{i(S_{EH}[g]+S_M[g,\phi_0])} \mathcal{N} \int D_\Lambda \delta\phi e^{i \int d^4x \frac{\delta\phi^2(x)}{2} \frac{\delta^2 S_M[g,\phi]}{\delta\phi^2(x)}|_{\phi=\phi_0} + \dots} \quad (\text{A.2})$$

where the path integral will have the usual perturbative renormalization. Hence, one can consider the physical observables to be defined through

$$T_{\mu\nu}(y) = \frac{2}{\sqrt{g(y)}} \frac{\delta}{\delta g^{\mu\nu}(y)} \left(S_M[g, \phi_0] - i \ln \left\{ \mathcal{N} \int D\Lambda \delta\phi \exp \left[i \int d^4x \frac{\delta\phi^2(x)}{2} \frac{\delta^2 S_M[g, \phi]}{\delta\phi^2(x)} \Big|_{\phi=\phi_0} + \dots \right] \right\} \right). \quad (\text{A.3})$$

Note that in practice, we are expanding $g_{\mu\nu}$ perturbatively about a homogeneous and isotropic FRW background before doing the path integral. Hence, the inhomogeneities can be computed using classical perturbation theory and the renormalization scale need not be at $\Lambda = H_{PT}$ even though it is at length scales longer than H_{PT}^{-1} for which homogeneity and isotropy are typically a good assumptions.

Appendix B: Derivation of Eq. (3.3)

Start with the thermally averaged Boltzmann equation for $n_X(t)$

$$\frac{1}{a^3} \frac{d}{dt} (n_X a^3) = -\langle\sigma v\rangle (n_X^2 - n_X^{\text{eq}2}) \quad (\text{B.1})$$

which says that n_X tracks the equilibrium number density n_X^{eq} until freeze out occurs at $t = t_f$. Long after freeze out, the equilibrium term can be neglected, and the equation asymptotically approaches

$$\frac{d}{dt} (n_X a^3) = -\langle\sigma v\rangle (n_X a^3)^2 \frac{1}{a^3}. \quad (\text{B.2})$$

One can solve for $n_X(t_0)$ by integrating

$$n_X(t_0) = \frac{n_X(t_f) \left(\frac{a_f}{a_0}\right)^3}{1 + n_X(t_f) \left(\frac{a_f}{a_0}\right)^3 \int_{t_f}^{t_0} dt \langle\sigma v\rangle \frac{a_0^3}{a^3}}. \quad (\text{B.3})$$

The integral in the denominator accounts for residual annihilations of dark matter particles after freeze out. The freeze out time t_f is not fundamental but instead an artifact of defining when the solution deviates “significantly” from the equilibrium distribution. For temperatures away from resonances and thresholds, one can typically parameterize $\langle\sigma v\rangle$ as

$$\langle\sigma v\rangle = \tilde{a} + \tilde{b} \frac{T}{m_X}, \quad (\text{B.4})$$

where T is the temperature and m_X is the mass of the dark matter. To further reduce Eq. (B.3) we apply Eq. (3.25), which implicitly defines t_f , and approximate $n_X(t_f) \approx n_X^{\text{eq}}(t_f)$. Then, the denominator of Eq. (B.3) satisfies

$$n_X(t_f) \left(\frac{a_f}{a_0}\right)^3 \int_{t_f}^{t_0} dt \langle\sigma v\rangle \frac{a_0^3}{a^3} \approx \frac{m_X}{T_f} \left(\frac{\tilde{a} + \frac{\tilde{b}}{2} \frac{T_f}{m_X}}{\tilde{a} + \tilde{b} \frac{T}{m_X}} \right) \gg 1 \quad (\text{B.5})$$

for $T_f \approx m_X/20$ the freeze out temperature. Using this approximation we can express the relic abundance as

$$n_X(t_0) = \left(\int_0^{\ln a_0/a_f} \frac{d \ln(a/a_f)}{H} \langle \sigma v \rangle \frac{a_0^3}{a^3} \right)^{-1} \quad (\text{B.6})$$

after also applying $dt = H^{-1} d \ln a$.

Appendix C: Difference Between Entropy and Energy Degrees of Freedom

In this appendix, we show that as the universe expands adiabatically during radiation domination, the relationship $g_E(T) = g_S(T)$ hold iff

$$\frac{d \ln g_E}{d \ln T} = \frac{d \ln g_S}{d \ln T} = 0 \quad (\text{C.1})$$

where g_E is the effective number of degrees of freedom for the thermal energy density and g_S is the effective number of degrees of freedom for the entropy density. We also justify an ansatz that can be used to relate g_E and g_S .

Assume that the CC energy density is negligible so that $\rho \approx \rho_R$, which is the case sufficiently far before or after the PT. The entropy and energy densities of a gas are related by Eq. (2.1c), which can be written as

$$\rho + P - T s = 0 \quad (\text{C.2})$$

where the pressure P of the gas is given by $P(T) = -\mathcal{F}(T)$. The functions g_E and g_S representing the number of relativistic degrees of freedom were defined by Eq. (3.9) and Eq. (3.10) and are reproduced here for convenience:

$$\rho = \frac{\pi^2}{30} g_E(T) T^4 \quad \text{and} \quad s = \frac{2\pi^2}{45} g_S(T) T^3. \quad (\text{C.3})$$

As the universe expands, energy conservation is enforced by

$$d(\rho a^3) + P da^3 = 0. \quad (\text{C.4})$$

Using Eq. (C.2) and Eq. (C.3) this becomes

$$\frac{d \ln g_E(T)}{d \ln a} + 4 \frac{d \ln T}{d \ln a} + 4 \frac{g_S}{g_E} = 0, \quad (\text{C.5})$$

which can be resolved as

$$\frac{d \ln T}{d \ln a} = -\frac{g_S}{g_E} \left[1 + \frac{1}{4} \frac{d \ln g_E(T)}{d \ln T} \right]^{-1}. \quad (\text{C.6})$$

Next, impose adiabaticity $d(sa^3)/da = 0$ by first using Eq. (C.3) to write

$$\frac{d \ln(sa^3)}{d \ln a} = - \left[\frac{d \ln g_S}{d \ln T} + 3 \right] \frac{g_S}{g_E} \left[1 + \frac{1}{4} \frac{d \ln g_E(T)}{d \ln T} \right]^{-1} + 3, \quad (\text{C.7})$$

and then setting this to zero and solving to find

$$\frac{g_S}{g_E} = 1 + \frac{1}{4} \frac{d \ln g_E}{d \ln T} - \frac{1}{3} \frac{d \ln g_S}{d \ln T}. \quad (\text{C.8})$$

This equation implies $g_E = g_S$ iff

$$\frac{d \ln g_E}{d \ln T} = \frac{d \ln g_S}{d \ln T} = 0 \quad (\text{C.9})$$

as claimed.

To obtain some intuition for this theorem consider the SM electroweak PT. Before the PT, the entire spectrum is massless and Eq. (C.9) is satisfied exactly so $g_E(T) = g_S(T) = \text{const}$ for $T > T_{PT}$. After the PT, we can estimate how much difference between g_S and g_E is required for self-consistency and to justify an intuitive parameterization, by considering a hypothetical situation in which one can approximate

$$g_{E/S}(T) = g_{E/S}(T_i) [T/T_i]^{-12K} \quad (\text{C.10})$$

where K is a constant and T_i is an initial condition temperature. Then, one can solve Eq. (C.8) as

$$\frac{g_S(T)}{g_E(T)} = \frac{1 - 3K}{1 - 4K}. \quad (\text{C.11})$$

Hence, if $0 < K \ll 1$, we have a situation in which $g_E(T)$ decreases slowly as a function of time while satisfying both entropy conservation and $g_S(T) \approx g_E(T)$. Presumably, K can be viewed as a leading term in a Taylor expansion regarding g_S/g_E . Hence, we will approximate

$$g_S(T) \approx (1 + K) g_E(T) \quad (\text{C.12})$$

even though we are not necessarily making the assumption of Eq. (C.10) throughout the paper.

Appendix D: Derivation of T_{PT}^+ , Δs , and $T(a)$

To find $T(a)$, we start with the temperature before the PT T_{PT}^- and impose energy conservation to solve for the temperature after the PT T_{PT}^+ . This allows us to calculate Δs and ϵ_2 in terms of $\Delta \rho_{\text{ex}}$. Then, we require the entropy per comoving volume $S = sa^3$ to be conserved before and after the PT to find $T(a)$.

Assuming that there is a negligible change in a during reheating, we can impose energy conservation at a_{PT} . Using Eqs. (2.6), (3.8), and (3.9), energy conservation can be written as

$$\frac{\pi^2}{30} g_E^{(s)}(T_{PT}^-) (T_{PT}^-)^4 + \Delta\rho_{\text{ex}} = \frac{\pi^2}{30} g_E^{(b)}(T_{PT}^+) (T_{PT}^+)^4, \quad (\text{D.1})$$

which implicitly defines T_{PT}^+ . This equation can be solved analytically by expanding $T_{PT}^+ = T_{PT}^- (1 + \Delta\tau)$ and linearizing in $\Delta\tau$ along with other small quantities. Using Eq. (3.15) to expand $g_E^{(s)}(T)$ around $g_E^{(s)}(T_f)$, Eq. (D.1) becomes

$$\frac{\pi^2}{30} \left[\lim_{\epsilon \rightarrow 0} h(a_{PT} + \epsilon) - h(a_{PT} - \epsilon) \right] (T_{PT}^-)^4 + \Delta\rho_{\text{ex}} \approx 4 \frac{\pi^2}{30} g_E^{(s)}(T_f) (T_{PT}^-)^4 \Delta\tau. \quad (\text{D.2})$$

where we have dropped higher order terms. Using Eq. (3.16), the term in brackets is $(7/8)N_{PT}$. Finally, the equation can be solved for $\Delta\tau = T_{PT}^+/T_{PT}^- - 1$ to obtain

$$T_{PT}^+ \approx T_{PT}^- \left[1 + \frac{1}{4} \epsilon_{31} + \frac{1}{4} \frac{\Delta\rho_{\text{ex}}}{\frac{\pi^2}{30} g_E^{(s)}(T_f) (T_{PT}^-)^4} \right] \quad (\text{D.3})$$

where ϵ_{31} is given by Eq. (3.20c). As expected, the energy released $\Delta\rho_{\text{ex}} > 0$ controls the reheating from T_{PT}^- to T_{PT}^+ . Additionally, the reheating is larger when more particles non-adiabatically decouple (larger ϵ_{31}), because the latent heat is distributed over fewer degrees of freedom after the PT.

Next we can calculate the entropy density increase at the PT given by

$$\Delta s \equiv s^{(b)}(T_{PT}^+) - s^{(s)}(T_{PT}^-) \quad (\text{D.4})$$

$$= \frac{2\pi^2}{45} \left\{ g_S^{(b)}(T_{PT}^+) (T_{PT}^+)^3 - g_S^{(s)}(T_{PT}^-) (T_{PT}^-)^3 \right\}. \quad (\text{D.5})$$

Once again we will linearize in the perturbation by expanding g_S using Eq. (3.15) and writing T_{PT}^+ using Eq. (D.3). This gives

$$\Delta s \approx \frac{2\pi^2}{45} \left\{ -\frac{1}{g_S^{(s)}(T_f)} \left[\lim_{\epsilon \rightarrow 0} h(a_{PT} + \epsilon) - h(a_{PT} - \epsilon) \right] + 3\Delta\tau \right\} g_S^{(s)}(T_f) (T_{PT}^-)^3 \quad (\text{D.6})$$

$$\approx \frac{2\pi^2}{45} \left\{ -\frac{g_E^{(s)}(T_f)}{g_S^{(s)}(T_f)} \epsilon_{31} + 3 \left[\frac{1}{4} \epsilon_{31} + \frac{1}{4} \frac{\Delta\rho_{\text{ex}}}{\frac{\pi^2}{30} g_E^{(s)}(T_f) (T_{PT}^-)^4} \right] \right\} g_S^{(s)}(T_f) (T_{PT}^-)^3 \quad (\text{D.7})$$

As discussed in Section C, we can approximate $g_S^{(s)}(T_f) \approx g_E^{(s)}(T_f)$. Then finally Δs becomes

$$\Delta s \approx \frac{2\pi^2}{45} g_S^{(s)}(T_f) (T_{PT}^-)^3 \left[-\frac{1}{4} \epsilon_{31} + \frac{1}{4} \frac{\Delta\rho_{\text{ex}}}{\frac{\pi^2}{30} g_E^{(s)}(T_f) (T_{PT}^-)^4} \right]. \quad (\text{D.8})$$

Using Eq. (3.20b) and noting $T_{PT}^- a_{PT} = T_f a_f$ up to higher order terms, we also obtain

$$\epsilon_2 \approx -\frac{1}{4} \epsilon_{31} + \frac{1}{4} \frac{\Delta \rho_{\text{ex}}}{\frac{\pi^2}{30} g_E^{(s)}(T_f) (T_{PT}^-)^4}. \quad (\text{D.9})$$

Both of these equations illustrate that the entropy increase at the PT is controlled by the amount of latent heat released and the number of particles that non-adiabatically decouple.

Finally we will solve the equation of entropy conservation for $T(a)$. The entropy per comoving volume $S = s a^3$ is conserved excepting the entropy injection at reheating which is assumed to occur rapidly at a_{PT} . Entropy conservation may be expressed as

$$g_S(a) T(a)^3 a^3 = g_S^{(s)}(T_f) T_f^3 a_f^3 + \Theta(a - a_{PT}) a_{PT}^3 \left(\frac{2\pi^2}{45} \right)^{-1} \Delta s, \quad (\text{D.10})$$

which implicitly defines $T(a)$. To solve for T we use Eq. (3.15) to expand $g_S(a)$ then linearize in h and Δs to obtain

$$T(a) \approx T_f \frac{a_f}{a} \left[1 + \frac{1}{3} \frac{h(a)}{g_S^{(s)}(T_f)} + \Theta(a - a_{PT}) \frac{1}{3} \left(\frac{a_{PT}}{a_f} \right)^3 \frac{\Delta s}{\frac{2\pi^2}{45} g_S^{(s)}(T_f) T_f^3} \right] \quad (\text{D.11})$$

Further expanding h using Eq. (3.16), approximating $g_S(T_f) \approx g_E(T_f)$, and applying Eq. (3.20b) we obtain the final expression,

$$T(a) \approx T_f \frac{a_f}{a} \left[1 + \frac{1}{3} \epsilon_{32} f(a) + \Theta(a - a_{PT}) \frac{1}{3} (\epsilon_{31} + \epsilon_2) \right] \quad (\text{D.12})$$

After the PT, the exotic energy component behaves approximately adiabatically.

Appendix E: Derivation of PT induced change in the degree of freedom

We begin with the well-known formula for the energy density of a gas of fermions at temperature T with N dynamical degrees of freedom:

$$\rho(T) = N \int \frac{d^3 p}{(2\pi)^3} \frac{E_p}{1 + e^{E_p/T}}. \quad (\text{E.1})$$

The gas has an effective number of degrees of freedom g_E given implicitly by $\rho(T) = \frac{\pi^2}{30} g_E(T) T^4$. We can parameterize the decrease in g_E due to the decoupling of the fermionic gas by writing

$$g_E(T) = g_E(T_f) - \frac{7}{8} N f(a/a_f) \quad (\text{E.2})$$

where

$$f(a) = \left(\frac{7\pi^2}{8 \cdot 30} \right)^{-1} \int \frac{d^3 p}{(2\pi)^3} E_p \left[\frac{1}{T_f^4} \frac{1}{e^{\frac{E_p}{T_f}} + 1} - \frac{1}{T^4(a)} \frac{1}{e^{\frac{E_p}{T(a)}} + 1} \right]. \quad (\text{E.3})$$

The temperature $T = T(a)$ is given by Eq. (D.12) to leading order in the perturbations ϵ_i . Since f already multiplies a small term in Eq. (3.16), we need only keep the leading factor in Eq. (D.12) which is $T = T_f a_f/a$. This lets us write Eq. (E.3) as

$$f(a) = \frac{8}{7} \left(\frac{30}{\pi^2} \right) \int \frac{d^3p}{(2\pi)^3} \frac{E_p}{T_f^4} \left[\frac{1}{e^{\frac{E_p}{T_f}} + 1} - \frac{(a/a_f)^4}{e^{\frac{aE_p}{a_f T_f}} + 1} \right]. \quad (\text{E.4})$$

Note that $f(a)$ increases from $f(a_f) = 0$ to $f(\infty) \approx 1$. Due to the exponential temperature dependence, the transition to $f \approx 1$ occurs at $T \approx m_N$ and is smoothly steplike over a time scale $\Delta t \approx 1/H$. In this discussion we have assumed $E_p = \sqrt{\mathbf{p}^2 + m_N^2}$ with m_N constant, that is, we neglect any change in the mass of the particle as a function of time. This assumption is valid sufficiently far after the PT such that the scalar field expectation value and field-dependent masses have approximately stopped varying.

Appendix F: Thermal Effective Potential Details

We have calculated the thermal effective potential through one-loop order for each of the models in Section 4. Our calculation employs the standard techniques [74–76], and the case of the Standard Model is particularly well documented [49, 77, 78]. As such, we do not feel the need to reproduce the entire calculation here. However, we have chosen to use renormalization schemes which are convenient for our calculation, but not standardly employed. Hence, we will use this appendix to write down the thermal effective potentials for each of the models in Section 4 and to spell out our renormalization conditions.

In calculating thermal corrections to the scalar effective potential, we do not include contributions from the dark matter sector. This is an excellent approximation provided that freeze out occurs prior to the phase transition (as we have assumed), such that the dark matter is decoupled from the plasma during the phase transition.

1. Thermal Effective Potential: Standard Model

Let $h(x) = \sqrt{2} |H^\dagger H|^{1/2}$ be the radial component of the SM Higgs field and let $h_c = \langle h \rangle$. In calculating the radiative corrections, we need not include the contributions from every field in the Standard Model. With regards to the non-thermal corrections, light particles which couple weakly to the Higgs can be neglected, and with regards to the thermal corrections, particles which are light

and do not decouple during freeze out can be treated as massless. Since we expect that freeze out will coincide with the PT at a mass scale of about 100 GeV and that residual annihilations will occur down to a mass scale of about 10 GeV, we can neglect particles with a mass below that of the bottom quark (i.e., 4.2 GeV). We retain the top quark, bottom quark, physical Higgs, and massive gauge bosons⁹ which have field dependent masses

$$M_{t/b/Z/W}^2(h_c) = \left(\frac{m_{t/b/Z/W}}{v} \right)^2 h_c^2 \quad (\text{F.1a})$$

$$M_h^2(h_c) = \frac{m_h^2}{2v^2} (3h_c^2 - v^2) \quad (\text{F.1b})$$

where $m_t = 172.6$ GeV, $m_b = 4.2$ GeV, $m_Z = 91.2$ GeV, and $m_W = 80.4$ GeV [79]. The non-thermal corrections can be expressed as functions of the Coleman-Weinberg potential [74]. Regulating in ($d = 4 - 2\epsilon$) spacetime dimensions, the unrenormalized potential is given by

$$V_{\text{cw}}(M^2) = \frac{M^4}{64\pi^2} \left(\log \frac{M^2}{\mu^2} - \frac{3}{2} - C_{\text{uv}} \right) \quad (\text{F.2})$$

where $C_{\text{uv}} = \epsilon^{-1} - \gamma_E + \ln 4\pi$ and μ is the t'Hooft scale. The thermal corrections can be expressed in terms of the bosonic and fermionic thermal functions [75, 80]

$$J_B(y) \equiv \int_0^\infty dx x^2 \log \left(1 - e^{-\sqrt{x^2+y}} \right) = - \sum_{n=1}^\infty \frac{1}{n^2} y K_2(n\sqrt{y}) \quad (\text{F.3a})$$

$$J_F(y) \equiv \int_0^\infty dx x^2 \log \left(1 + e^{-\sqrt{x^2+y}} \right) = - \sum_{n=1}^\infty \frac{(-1)^n}{n^2} y K_2(n\sqrt{y}) \quad (\text{F.3b})$$

where $K_2(z)$ is the modified Bessel function of the second kind. Putting the pieces together, the Standard Model thermal effective potential (through one-loop order and before renormalization) is given by

$$\begin{aligned} V_{\text{eff}}^{(\text{SM})}(h_c, T) \approx & \frac{m_h^2}{8v^2} (h_c^2 - v^2)^2 + \left\{ \delta\Omega + \frac{1}{2} \delta m^2 h_c^2 + \frac{\delta\lambda}{4} h_c^4 \right. \\ & - 12 V_{\text{cw}}(M_t^2(h_c)) - 12 V_{\text{cw}}(M_b^2(h_c)) + 3 V_{\text{cw}}(M_Z^2(h_c)) + 6 V_{\text{cw}}(M_W^2(h_c)) + V_{\text{cw}}(M_h^2(h_c)) \Big\} \\ & + \left\{ -\frac{\pi^2}{90} 75.75 T^4 + \frac{T^4}{2\pi^2} \left[-12 J_F(M_t^2(h_c) T^{-2}) - 12 J_F(M_b^2(h_c) T^{-2}) \right. \right. \\ & \left. \left. + 3 J_B(M_Z^2(h_c) T^{-2}) + 6 J_B(M_W^2(h_c) T^{-2}) + J_B(M_h^2(h_c) T^{-2}) \right] \right\} + O(\hbar^2) \quad (\text{F.4}) \end{aligned}$$

⁹ We work in the Landau gauge ($\xi = 0$) for which the scalar polarization mode and ghost propagators are independent of h_c [74].

where $\delta\Omega$, δm^2 , and $\delta\lambda$ are counterterms. We have also included the term $(-\frac{\pi^2}{90}75.75 T^4)$, which represents the thermal radiative contribution from light quarks, leptons, and massless gauge bosons which are relativistic at temperatures $T \gtrsim 10$ GeV. The renormalization conditions,

$$\left. \frac{\partial}{\partial h_c} V_{\text{eff}}^{(\text{SM})}(h_c, 0) \right|_{h_c=v} = 0 \quad (\text{F.5a})$$

$$\left. \frac{\partial^2}{\partial h_c^2} V_{\text{eff}}^{(\text{SM})}(h_c, 0) \right|_{h_c=v} = m_h^2 \quad (\text{F.5b})$$

$$V_{\text{eff}}^{(\text{SM})}(v, 0) = 0, \quad (\text{F.5c})$$

are chosen such that tadpole graphs vanish and $V_{\text{eff}}^{(\text{SM})}(h_c, 0)$ has a minimum at $h_c = v$, self-energy graphs vanish and the Higgs mass¹⁰ is m_h , and the CC is tuned against the vacuum energy density to zero.

2. Thermal Effective Potential: \mathbb{Z}_2 xSM

The \mathbb{Z}_2 xSM potential was specified by Eq. (4.8). Since we focus on the case $\langle s \rangle = 0$, we need only calculate the effective potential as a function of h_c and not $s_c = \langle s \rangle$. That is, the presence of the singlet in this model simply add an additional degree of freedom, with field dependent mass

$$M_s^2(h_c) = (m_s^2 - a_2 v^2) + a_2 h_c^2, \quad (\text{F.6})$$

to the radiative corrections. We can construct the effective potential from the SM effective potential Eq. (F.4) as

$$V_{\text{eff}}^{(\mathbb{Z}_2\text{xSM})}(h_c, T) = V_{\text{eff}}^{(\text{SM})}(h_c, T) + V_{\text{cw}}(M_s^2(h_c)) + \frac{T^4}{2\pi^2} J_B(M_s^2(h_c)T^{-2}). \quad (\text{F.7})$$

An additional UV divergence arises from the term $V_{\text{cw}}(M_s^2)$, and is cancelled by solving the renormalization conditions Eq. (F.5) once again for the counterterms.

3. Thermal Effective Potential: Generic Singlet

For the theory specified by the action Eq. (4.13), we have the field dependent masses

$$M_\varphi^2(\varphi_c) = M^2 - 6\mathcal{E}\varphi_c + 3\lambda\varphi_c \quad (\text{F.8})$$

$$M_{\psi_i}^2(\varphi_c) = (m_i + h_i\varphi_c)^2. \quad (\text{F.9})$$

¹⁰ Since the effective potential is computed from diagrams with zero external momentum, the mass $\partial_{h_c}^2 V_{\text{eff}}(h_c = v, 0) = m_h^2$ differs from the Higgs pole mass by logarithmic corrections [81], which we verify are $O(\text{few } \%)$. As such, we will neglect this distinction and continue to refer to m_h as the ‘‘Higgs mass.’’

We construct the thermal effective potential as

$$V_{\text{eff}}^{(\text{GS})}(\varphi_c, T) = \rho_{\text{ex}} + \frac{1}{2}M^2\varphi_c^2 - \mathcal{E}\varphi_c^3 + \frac{\lambda}{4}\varphi_c^4 + \frac{T^4}{2\pi^2} \left[J_B(M_\varphi^2(\varphi_c)) - 4 \sum_{i=1}^N J_F(M_{\psi_i}^2(\varphi_c)) \right] \quad (\text{F.10})$$

$$+ \left\{ \delta\Omega + \delta t \varphi_c + \frac{1}{2}\delta M^2\varphi_c^2 - \delta\mathcal{E}\varphi_c^3 + \frac{\delta\lambda}{4}\varphi_c^4 + V_{\text{cw}}(M_\varphi^2(\varphi_c)) - 4 \sum_{i=1}^N V_{\text{cw}}(M_{\psi_i}^2(\varphi_c)) \right\}$$

where $\delta\Omega$, δt , δM^2 , $\delta\mathcal{E}$, and $\delta\lambda$ are counterterms. We do not renormalize using the same renormalization conditions as we did for the SM. To simplify the discussions of Section 4, we have attempted to choose the renormalization conditions such that the effective potential preserves certain features of the renormalized tree-level potential. For example, the renormalization conditions that we applied to the SM, Eq. (F.5), ensured that the effective potential and the tree-level potential agreed to order h_c^2 as an expansion around $h_c = v$. In our analysis of Section 4.3, we found it convenient to define the parameter α_0 which controls the shape of the effective potential. This parameter is defined using the tree-level potential $U(\varphi)$, but we claim that it also describes the shape of the one-loop effective potential provided that the radiative corrections do not significantly distort the shape of the potential. For the tuned limit $0 \lesssim \alpha_0 \ll 1$, this parameter is particularly sensitive to the shape of the potential near the origin $\varphi_c = 0$ since the barrier is very small. The radiative corrections grow as $\varphi_c \rightarrow 0$, because the fermions ψ_i become light, but these logarithmic corrections remain subdominant. However, with a renormalization scheme of the form of Eq. (F.5), the counterterms pick up a finite piece, which depends on derivatives of logarithms at the renormalization point $\varphi_c \approx v$, and which contributes non-negligibly near $\varphi_c \approx 0$. If we were to use such a renormalization scheme in the limit where $U(\varphi_c)$ has a small barrier so $0 \lesssim \alpha_0 \ll 1$, then the radiative corrections may lift the minimum at $\varphi_c \approx 0$ and eliminate the barrier. Of course, there is nothing incorrect with using such a renormalization scheme except that it is inconvenient since we would not be able to characterize the shape of the potential using α_0 derived from $U(\varphi_c)$.

In light of this discussion, we will use a renormalization scheme which preserves the location of the minimum at $\varphi_c = v$ and also preserves the shape of the potential near $\varphi_c = 0$. This is accomplished by first writing Eq. (F.10) for $T = 0$ as

$$V_{\text{eff}}^{(\text{GS})}(\varphi_c, 0) = \bar{\Omega}(\varphi_c) + \bar{t}(\varphi_c)\varphi_c + \frac{1}{2}\bar{M}^2(\varphi_c)\varphi_c^2 - \bar{\mathcal{E}}(\varphi_c)\varphi_c^3 + \frac{\bar{\lambda}(\varphi_c)}{4}\varphi_c^4 \quad (\text{F.11})$$

where

$$\bar{\Omega}(\varphi_c) = \rho_{\text{ex}} + \delta\Omega + \frac{\hbar}{4\pi^2} \left[\frac{1}{16} M^4 f_\varphi(\varphi_c) - \frac{1}{4} \sum_{i=1}^N m_i^4 f_{\psi_i}(\varphi_c) \right] \quad (\text{F.12a})$$

$$\bar{t}(\varphi_c) = \delta t + \frac{\hbar}{4\pi^2} \left[-\frac{3}{4} \mathcal{E} M^2 f_\varphi(\varphi_c) - \sum_{i=1}^N m_i^3 h_i f_{\psi_i}(\varphi_c) \right] \quad (\text{F.12b})$$

$$\bar{M}^2(\varphi_c) = M^2 + \delta M^2 + \frac{\hbar}{4\pi^2} \left[\frac{3}{4} M^2 \lambda f_\varphi(\varphi_c) + \frac{9}{2} \mathcal{E}^2 f_\varphi(\varphi_c) - 3 \sum_{i=1}^N m_i^2 h_i^2 f_{\psi_i}(\varphi_c) \right] \quad (\text{F.12c})$$

$$\bar{\mathcal{E}}(\varphi_c) = \mathcal{E} + \delta\mathcal{E} + \frac{\hbar}{4\pi^2} \left[\frac{9}{4} \mathcal{E} \lambda f_\varphi(\varphi_c) + \sum_{i=1}^N m_i h_i^3 f_{\psi_i}(\varphi_c) \right] \quad (\text{F.12d})$$

$$\bar{\lambda}(\varphi_c) = \lambda + \delta\lambda + \frac{\hbar}{4\pi^2} \left[\frac{9}{4} \lambda^2 f_\varphi(\varphi_c) - \sum_{i=1}^N h_i^4 f_{\psi_i}(\varphi_c) \right] \quad (\text{F.12e})$$

and

$$f_\varphi(\varphi_c) = \left(\ln \frac{M_\varphi^2(\varphi_c)}{\mu^2} - \frac{3}{2} - C_{\text{uv}} \right) \quad (\text{F.13})$$

$$f_{\psi_i}(\varphi_c) = \left(\ln \frac{M_{\psi_i}^2(\varphi_c)}{\mu^2} - \frac{3}{2} - C_{\text{uv}} \right). \quad (\text{F.14})$$

Then the renormalization conditions can be expressed as

$$\bar{\Omega}(v) = \rho_{\text{ex}} \quad (\text{F.15a})$$

$$\bar{t}(v) = 0 \quad (\text{F.15b})$$

$$\bar{M}^2(v) = M^2 \quad (\text{F.15c})$$

$$\bar{\mathcal{E}}(v) = \mathcal{E} \quad (\text{F.15d})$$

$$\bar{\lambda}(v) = \lambda. \quad (\text{F.15e})$$

Near $\varphi_c \approx 0$, the radiative corrections are at most logarithmic.

4. Thermal Effective Potential: xSM

In Section 4.4 we wrote down the xSM renormalized potential in Eq. (4.34). For general h_c and s_c , the Higgs and singlet fields mix. In order to calculate the radiative corrections, we must generalize the field-dependent Higgs mass M_h^2 , given by Eq. (F.1b), to the Higgs-singlet mass matrix

M_{hs}^2 , which has components

$$[M_{hs}^2(\{h_c, s_c\})]_{11} = m_h^2/(2v^2) (3h_c^2 - v^2) + s_c (a_1 + a_2 s_c) \quad (\text{F.16a})$$

$$[M_{hs}^2(\{h_c, s_c\})]_{12} = [M_{hs}^2(\{h_c, s_c\})]_{21} = h_c (a_1 + 2 a_2 s_c) \quad (\text{F.16b})$$

$$[M_{hs}^2(\{h_c, s_c\})]_{22} = m_s^2 + a_2 (h_c^2 - v^2) + 2b_3 s_c + 3b_4 s_c^2. \quad (\text{F.16c})$$

Now we can write down the thermal effective potential in terms of $V_{\text{eff}}^{(\text{SM})}$ by subtracting the contribution from the SM Higgs and adding the contribution from the mixed Higgs and singlet. Doing so we obtain

$$\begin{aligned} V_{\text{eff}}^{(\text{xSM})}(\{h_c, s_c\}, T) = & V_{\text{eff}}^{(\text{SM})}(h_c, T) + \frac{b_4}{4} s_c^4 + \frac{1}{2} m_s^2 s_c^2 + \frac{b_3}{3} s_c^3 + \frac{1}{2} s_c (h_c^2 - v^2) (a_1 + a_2 s_c) \\ & + \left\{ \frac{\delta b_4}{4} s_c^4 + \frac{\delta b_3}{3} s_c^3 + \frac{1}{2} \delta b_2 s_c^2 + \delta b_1 s_c + \frac{1}{2} \delta a_2 s_c^2 h_c^2 + \frac{1}{2} \delta a_1 s_c h_c^2 + \delta \Omega \right. \\ & \left. - V_{\text{cw}}(M_h^2(h_c)) + \text{Tr } V_{\text{cw}}(M_{hs}^2(\{h_c, s_c\})) \right\} \\ & + \frac{T^4}{2\pi^2} [-J_B(M_h^2(h_c)T^{-2}) + \text{Tr } J_B(M_{hs}^2(\{h_c, s_c\})T^{-2})] \end{aligned} \quad (\text{F.17})$$

where $\delta\Omega$, δb_i , and δa_i are counterterms. The trace is interpreted to mean evaluating V_{cw} or J_B with the eigenvalues of M_{hs}^2 . We generalize the SM renormalization conditions Eq. (F.5) to incorporate the additional fields,

$$\begin{aligned} \left(\frac{\partial}{\partial h_c} \right)^{n_h} \left(\frac{\partial}{\partial s_c} \right)^{n_s} V_{\text{eff}}^{(\text{xSM})}(\{h_c, s_c\}) \Big|_{\{v,0\}} &= \left(\frac{\partial}{\partial h_c} \right)^{n_h} \left(\frac{\partial}{\partial s_c} \right)^{n_s} U(\{h_c, s_c\}) \Big|_{\{v,0\}} \\ \{n_h, n_s\} &= \{1, 0\}, \{2, 0\}, \{0, 1\}, \{0, 2\}, \{1, 1\}, \{1, 2\}, \{0, 3\}, \{0, 4\}, \{0, 0\} \end{aligned} \quad (\text{F.18})$$

where $U(\{h_c, s_c\})$ is given by Eq. (4.34). Once again, we require $V_{\text{eff}}^{(\text{xSM})}(\{v, 0\}, 0) = 0$ which tunes the CC.

Appendix G: xSM Bounce Calculation

As discussed in Section 4.4, the xSM electroweak PT is first order in the parametric regime of interest and proceeds through thermal bubble nucleation. In order to determine the bubble nucleation temperature T_{PT}^- we estimate the action of the three dimensional bounce $S^{(3)}(T)$ and require $S^{(3)}/T|_{T_{PT}^-} \sim 140$. The bounce field configuration $\phi_B(r)$ is a saddle point solution of the Euclidean equation of motion with an $O(3)$ symmetry. Let $\vec{\phi} = \{h, s\}$ be the field space coordinate

and let $\vec{\phi}_{sym} = v^{(s)}(T)$ and $\vec{\phi}_{brk} = v^{(b)}(T)$ be the location of the symmetric and broken phases at temperature T . In this notation, the field equation and boundary conditions can be written as

$$\frac{d^2 \vec{\phi}}{dr^2} + \frac{2}{r} \frac{d\vec{\phi}}{dr} - \vec{\nabla}_{\vec{\phi}} V_{\text{eff}}(\vec{\phi}, T) = 0 \quad (\text{G.1})$$

$$\left. \frac{d\vec{\phi}}{dr} \right|_{r=0} = 0, \quad \lim_{r \rightarrow \infty} \vec{\phi}(r) = \vec{\phi}_{sym} \quad (\text{G.2})$$

where r is the radial coordinate and V_{eff} is the thermal effective potential. The bounce solution is a curve $\vec{\phi}_B(r)$ which starts nearby to $\vec{\phi}_{brk}$ at $r = 0$ and approaches $\vec{\phi}_{sym}$ as $r \rightarrow \infty$. Once the solution $\vec{\phi}_B(r)$ is obtained, the bounce action is calculated as

$$S^{(3)}(T) = 4\pi \int_0^\infty r^2 dr \left[\frac{1}{2} \left(\frac{d\vec{\phi}_B}{dr} \right)^2 + V_{\text{eff}}(\vec{\phi}_B(r), T) \right]. \quad (\text{G.3})$$

It is difficult to solve Eq. (G.1) by brute force numerics, because the solution is unstable to perturbations about the initial point $\vec{\phi}_B(0)$, and the over shoot / under shoot method is non-trivial to apply in two dimensions.

Profumo et. al. [59] have outlined a numerical procedure which reduces the calculation to iteratively solving the one-dimensional analog of Eq. (G.1). They suggest that one should decompose the field equation into a basis with unit vectors parallel and perpendicular to the solution curve $\vec{\phi}(r)$. Suppose that there exists a curve $\vec{\phi}(x)$ that interpolates between $\vec{\phi}(0) = \vec{\phi}_{sym}$ and $\vec{\phi}(L) = \vec{\phi}_{brk}$. Let

$$x = \int_{\vec{\phi}_{sym}}^{\vec{\phi}(x)} |d\vec{\phi}| \quad (\text{G.4})$$

be the distance along the curve such that L is the total length and

$$\hat{e}_{\parallel} = \frac{d\vec{\phi}}{dx} \quad \text{and} \quad \hat{e}_{\perp} = \begin{pmatrix} 0 & 1 \\ -1 & 0 \end{pmatrix} \frac{d\vec{\phi}}{dx} \quad (\text{G.5})$$

are the unit vectors parallel and perpendicular to the curve at x . In this basis, Eq. (G.1) becomes

$$\left\{ \frac{d^2 x}{dr^2} + \frac{2}{r} \frac{dx}{dr} - \frac{dV(\vec{\phi}(x))}{dx} \right\} \hat{e}_{\parallel} = 0 \quad (\text{G.6})$$

$$\left\{ \left| \frac{d^2 \vec{\phi}}{dx^2} \right| \left(\frac{dx}{dr} \right)^2 - \left(\vec{\nabla}_{\vec{\phi}} V \right)_{\perp} \right\} \hat{e}_{\perp} = 0. \quad (\text{G.7})$$

The authors of [59] solve these equations numerically using an iterative procedure.

Since we compute T_{PT}^- by calculating the bounce at various temperatures in order to solve $S^{(3)}/T \approx 140$, the iterative procedure is too computationally intensive for our purposes. Fortunately,

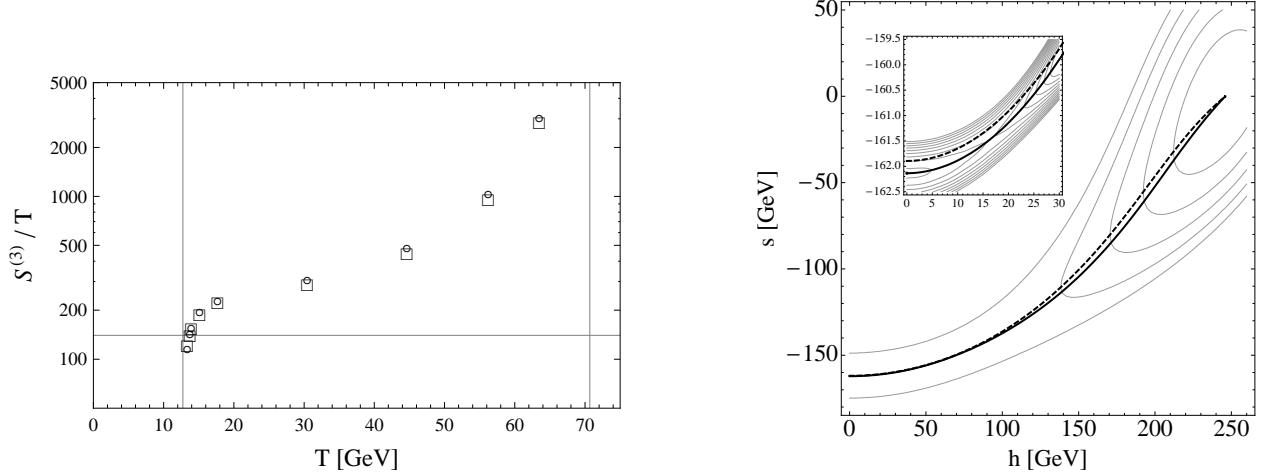


Figure 10: Comparisons of bounce calculations for the xSM benchmark point Eq. (4.37). On the left, the bounce action computed at various temperatures between $T_0 = 12.7$ GeV and $T_c = 70.7$ GeV using the method of [59] (squares) and our approximation (circles). On the right, the xSM thermal effective potential at $T_{PT}^- = 13.7$ GeV. The solid curve shows the trajectory $\vec{\phi}_B(x)$ obtained using the method of [59], and the dashed curve shows the approximation $\vec{\phi}_{\text{app}}(x)$ given by Eq. (G.8). The curves do not coincide at small h because the minimum along the $h = 0$ axis shifts as the temperature is raised. Nevertheless, the action along the two paths still agrees remarkably well.

in the parametric regime of interest the bounce solution $\vec{\phi}_B(r)$ can be approximated by $\vec{\phi}_{\text{app}}(x) = \{h(x), \bar{s}(h(x))\}$ where $\bar{s}(h)$ satisfies¹¹

$$\left. \frac{dU(\{h, s\}, 0)}{ds} \right|_{\bar{s}} = 0 \quad \text{and} \quad \bar{s}(v) = 0, \quad (\text{G.8})$$

U is the classical potential, and $\vec{\phi}_{\text{app}}(x)$ is parametrized by its length x given by Eq. (G.4). Using $\vec{\phi}_{\text{app}}(x)$, we solve Eq. (G.6) for $x(r)$ and calculate $S^{(3)}$ using Eq. (G.3).

To check our approximation, we also compute the PT temperature using the method of [59] for a few parameter sets. In Figure 10 we contrast our approximation with the procedure of [59] for the xSM benchmark point Eq. (4.37). We find that our approximation tends to overestimate $S^{(3)}$ by a few percent generically. However, $S^{(3)}$ is a rapidly increasing function of temperature, and even an $O(5\%)$ deviation in $S^{(3)}$ does not cause T_{PT}^- to deviate appreciably.

¹¹ In the parametric region described in Section 4.4, the solution of $dU/ds = 0$ is not generally a single-valued function of h . However, the boundary condition $\bar{s}(v) = 0$ selects out a unique trajectory which tends to stay in the “valley” connecting the two minima and passes through the saddle point.

Acknowledgments

We thank Lisa Everett, Lian-Tao Wang, and Sean Tulin for useful correspondence. DJHC thanks the hospitality of KIAS where part of this work was completed. DJHC and AJL were supported in part by the DOE through grant DE-FG02-95ER40896.

-
- [1] A. D. Linde, *Is the Lee Constant a Cosmological Constant?*, *JETP Lett.* **19** (1974) 183.
 - [2] J. R. Ellis, M. K. Gaillard, and D. V. Nanopoulos, *A Phenomenological Profile of the Higgs Boson*, *Nucl. Phys.* **B106** (1976) 292.
 - [3] J. Polchinski, *The Cosmological Constant and the String Landscape*, [hep-th/0603249](#).
 - [4] H. P. Nilles, *Supersymmetry, Supergravity and Particle Physics*, *Phys.Rept.* **110** (1984) 1–162.
 - [5] S. Weinberg, *The Cosmological Constant Problem*, *Rev.Mod.Phys.* **61** (1989) 1–23. Morris Loeb Lectures in Physics, Harvard University, May 2, 3, 5, and 10, 1988.
 - [6] D. A. Kirzhnits, *Weinberg Model in the Hot Universe*, *JETP Lett.* **15** (1972) 529–531.
 - [7] D. A. Kirzhnits and A. D. Linde, *Macroscopic Consequences of the Weinberg Model*, *Phys. Lett.* **B42** (1972) 471–474.
 - [8] E. W. Kolb and S. Wolfram, *Spontaneous Symmetry Breaking and the Expansion Rate of the Early Universe*, *Astrophys. J.* **239** (1980) 428.
 - [9] D. J. H. Chung, A. J. Long, and L.-T. Wang, *Probing the Cosmological Constant and Phase Transitions with Dark Matter*, [arXiv:1104.5034](#).
 - [10] R. A. Alpher, J. W. Follin, and R. C. Herman, *Physical Conditions in the Initial Stages of the Expanding Universe*, *Phys.Rev.* **92** (1953) 1347–1361.
 - [11] J. D. Barrow, *MASSIVE PARTICLES AS A PROBE OF THE EARLY UNIVERSE*, *Nucl.Phys.* **B208** (1982) 501–508.
 - [12] E. W. Kolb and M. S. Turner, *The Early universe*, *Front.Phys.* **69** (1990) 1–547.
 - [13] M. Kamionkowski and M. S. Turner, *THERMAL RELICS: DO WE KNOW THEIR ABUNDANCES?*, *Phys.Rev.* **D42** (1990) 3310–3320.
 - [14] P. Salati, *Quintessence and the relic density of neutralinos*, *Phys.Lett.* **B571** (2003) 121–131, [[astro-ph/0207396](#)].
 - [15] S. Aslanbeigi, G. Robbers, B. Z. Foster, K. Kohri, and N. Afshordi, *Phenomenology of Gravitational Aether as a solution to the Old Cosmological Constant Problem*, [arXiv:1106.3955](#). * Temporary entry *.
 - [16] N. Agarwal, R. Bean, J. Khoury, and M. Trodden, *Screening bulk curvature in the presence of large brane tension*, *Phys.Rev.* **D83** (2011) 124004, [[arXiv:1102.5091](#)].

- [17] C. de Rham, G. Gabadadze, L. Heisenberg, and D. Pirtskhalava, *Cosmic Acceleration and the Helicity-0 Graviton*, *Phys.Rev.* **D83** (2011) 103516, [[arXiv:1010.1780](#)].
- [18] L. Smolin, *The Quantization of unimodular gravity and the cosmological constant problems*, *Phys.Rev.* **D80** (2009) 084003, [[arXiv:0904.4841](#)].
- [19] C. Wetterich, *Warping with dilatation symmetry and self-tuning of the cosmological constant*, *Phys.Rev.* **D81** (2010) 103508, [[arXiv:1003.3809](#)].
- [20] J. E. Kim, *Self-tuning of the cosmological constant*, *J.Phys.Conf.Ser.* **259** (2010) 012005, [[arXiv:1009.5071](#)].
- [21] A. Davidson and S. Rubin, *Zero Cosmological Constant from Normalized General Relativity*, *Class.Quant.Grav.* **26** (2009) 235019, [[arXiv:0905.0661](#)].
- [22] P. Koroteev and M. Libanov, *On Existence of Self-Tuning Solutions in Static Braneworlds without Singularities*, *JHEP* **0802** (2008) 104, [[arXiv:0712.1136](#)].
- [23] F. Klinkhamer and G. Volovik, *Self-tuning vacuum variable and cosmological constant*, *Phys.Rev.* **D77** (2008) 085015, [[arXiv:0711.3170](#)].
- [24] G. Dvali, S. Hofmann, and J. Khoury, *Degravitation of the cosmological constant and graviton width*, *Phys.Rev.* **D76** (2007) 084006, [[hep-th/0703027](#)].
- [25] N. Itzhaki, *A Comment on Technical Naturalness and the Cosmological Constant*, *JHEP* **0608** (2006) 020, [[hep-th/0604190](#)].
- [26] H. M. Lee, *A Comment on the selftuning of cosmological constant with deficit angle on a sphere*, *Phys.Lett.* **B587** (2004) 117–120, [[hep-th/0309050](#)].
- [27] S. Kachru, M. B. Schulz, and E. Silverstein, *Selftuning flat domain walls in 5-D gravity and string theory*, *Phys.Rev.* **D62** (2000) 045021, [[hep-th/0001206](#)].
- [28] M. Quiros, *Finite Temperature Feld Theory and Phase Transitions*, [hep-ph/9901312](#).
- [29] R. R. Caldwell and M. Kamionkowski, *The Physics of Cosmic Acceleration*, *Ann.Rev.Nucl.Part.Sci.* **59** (2009) 397–429, [[arXiv:0903.0866](#)]. * Brief entry *.
- [30] E. Komatsu *et. al.*, *Seven-Year Wilkinson Microwave Anisotropy Probe (WMAP) Observations: Cosmological Interpretation*, [arXiv:1001.4538](#).
- [31] T. Cohen, D. E. Morrissey, and A. Pierce, *Changes in Dark Matter Properties After Freeze-Out*, *Phys. Rev.* **D78** (2008) 111701, [[arXiv:0808.3994](#)].
- [32] J. L. Feng, M. Kaplinghat, H. Tu, and H.-B. Yu, *Hidden Charged Dark Matter*, *JCAP* **0907** (2009) 004, [[arXiv:0905.3039](#)].
- [33] A. D. Linde, *Decay of the False Vacuum at Finite Temperature*, *Nucl. Phys.* **B216** (1983) 421.
- [34] E. Witten, *Cosmic Separation of Phases*, *Phys. Rev.* **D30** (1984) 272–285.
- [35] C. Wainwright and S. Profumo, *The Impact of a Strongly First-Order Phase Transition on the Abundance of Thermal Relics*, *Phys. Rev.* **D80** (2009) 103517, [[arXiv:0909.1317](#)].
- [36] F. Rosati, *Quintessential enhancement of dark matter abundance*, *Phys.Lett.* **B570** (2003) 5–10,

- [hep-ph/0302159].
- [37] S. Profumo and P. Ullio, *SUSY dark matter and quintessence*, *JCAP* **0311** (2003) 006, [hep-ph/0309220].
- [38] C. Pallis, *Quintessential kination and cold dark matter abundance*, *JCAP* **0510** (2005) 015, [hep-ph/0503080].
- [39] D. J. Chung, L. L. Everett, K. Kong, and K. T. Matchev, *Connecting LHC, ILC, and Quintessence*, *JHEP* **0710** (2007) 016, [arXiv:0706.2375].
- [40] D. J. Chung, L. L. Everett, and K. T. Matchev, *Inflationary cosmology connecting dark energy and dark matter*, *Phys.Rev.* **D76** (2007) 103530, [arXiv:0704.3285].
- [41] S. Weinberg, *Cosmological Constraints on the Scale of Supersymmetry Breaking*, *Phys.Rev.Lett.* **48** (1982) 1303.
- [42] G. Coughlan, W. Fischler, E. W. Kolb, S. Raby, and G. G. Ross, *Cosmological Problems for the Polonyi Potential*, *Phys.Lett.* **B131** (1983) 59.
- [43] J. McDonald, *WIMP Densities in Decaying-Particle-Dominated Cosmology*, *Phys. Rev.* **D43** (1991) 1063–1068.
- [44] T. Banks, D. B. Kaplan, and A. E. Nelson, *Cosmological implications of dynamical supersymmetry breaking*, *Phys.Rev.* **D49** (1994) 779–787, [hep-ph/9308292].
- [45] T. Moroi and L. Randall, *Wino cold dark matter from anomaly mediated SUSY breaking*, *Nucl.Phys.* **B570** (2000) 455–472, [hep-ph/9906527].
- [46] M. Berkooz, D. J. Chung, and T. Volansky, *Constraining modular inflation in the MSSM from giant Q-ball formation*, *Phys.Rev.* **D73** (2006) 063526, [hep-ph/0507218].
- [47] M. Dine, R. Kitano, A. Morisse, and Y. Shirman, *Moduli decays and gravitinos*, *Phys.Rev.* **D73** (2006) 123518, [hep-ph/0604140].
- [48] B. S. Acharya, P. Kumar, K. Bobkov, G. Kane, J. Shao, *et. al.*, *Non-thermal Dark Matter and the Moduli Problem in String Frameworks*, *JHEP* **0806** (2008) 064, [arXiv:0804.0863].
- [49] P. Arnold and O. Espinosa, *The Effective Potential and First Order Phase Transitions: Beyond Leading-Order*, *Phys. Rev.* **D47** (1993) 3546–3579, [hep-ph/9212235].
- [50] K. Kajantie, M. Laine, K. Rummukainen, and M. E. Shaposhnikov, *Is there a hot electroweak phase transition at $m(H) > \text{approx. } m(W)$?*, *Phys. Rev. Lett.* **77** (1996) 2887–2890, [hep-ph/9605288].
- [51] K. Kajantie, M. Laine, K. Rummukainen, and M. E. Shaposhnikov, *A non-perturbative analysis of the finite T phase transition in $SU(2) \times U(1)$ electroweak theory*, *Nucl. Phys.* **B493** (1997) 413–438, [hep-lat/9612006].
- [52] K. Kajantie, M. Laine, K. Rummukainen, and M. E. Shaposhnikov, *The Electroweak Phase Transition: A Non-Perturbative Analysis*, *Nucl. Phys.* **B466** (1996) 189–258, [hep-lat/9510020].
- [53] M. Gonderinger, Y. Li, H. Patel, and M. J. Ramsey-Musolf, *Vacuum Stability, Perturbativity, and Scalar Singlet Dark Matter*, *JHEP* **01** (2010) 053, [arXiv:0910.3167].

- [54] V. Barger, P. Langacker, M. McCaskey, M. J. Ramsey-Musolf, and G. Shaughnessy, *LHC Phenomenology of an Extended Standard Model with a Real Scalar Singlet*, *Phys. Rev.* **D77** (2008) 035005, [[arXiv:0706.4311](#)].
- [55] J. McDonald, *Gauge Singlet Scalars as Cold Dark Matter*, *Phys. Rev.* **D50** (1994) 3637–3649, [[hep-ph/0702143](#)].
- [56] C. P. Burgess, M. Pospelov, and T. ter Veldhuis, *The Minimal Model of Nonbaryonic Dark Matter: A Singlet Scalar*, *Nucl. Phys.* **B619** (2001) 709–728, [[hep-ph/0011335](#)].
- [57] X.-G. He, T. Li, X.-Q. Li, and H.-C. Tsai, *Scalar Dark Matter Effects in Higgs and Top Quark Decays*, *Mod. Phys. Lett.* **A22** (2007) 2121–2129, [[hep-ph/0701156](#)].
- [58] H. Davoudiasl, R. Kitano, T. Li, and H. Murayama, *The New Minimal Standard Model*, *Phys. Lett.* **B609** (2005) 117–123, [[hep-ph/0405097](#)].
- [59] S. Profumo, L. Ubaldi, and C. Wainwright, *Singlet Scalar Dark Matter: Monochromatic Gamma Rays and Metastable Vacua*, [arXiv:1009.5377](#).
- [60] F. Csikor, Z. Fodor, and J. Heitger, *Endpoint of the hot electroweak phase transition*, *Phys. Rev. Lett.* **82** (1999) 21–24, [[hep-ph/9809291](#)].
- [61] S. Profumo, M. J. Ramsey-Musolf, and G. Shaughnessy, *Singlet Higgs Phenomenology and the Electroweak Phase Transition*, *JHEP* **08** (2007) 010, [[arXiv:0705.2425](#)].
- [62] W. H. Miller, *Quantum mechanical transition state theory and a new semiclassical model for reaction rate constants*, *J. Chem. Phys.* **61** (1974) 1823.
- [63] A. D. Linde, *On the Vacuum Instability and the Higgs Meson Mass*, *Phys. Lett.* **B70** (1977) 306.
- [64] S. R. Coleman, *The Fate of the False Vacuum. 1. Semiclassical Theory*, *Phys. Rev.* **D15** (1977) 2929–2936.
- [65] C. G. Callan and S. R. Coleman, *The Fate of the False Vacuum. 2. First Quantum Corrections*, *Phys. Rev.* **D16** (1977) 1762–1768.
- [66] M. Dine, R. G. Leigh, P. Y. Huet, A. D. Linde, and D. A. Linde, *Towards the Theory of the Electroweak Phase Transition*, *Phys. Rev.* **D46** (1992) 550–571, [[hep-ph/9203203](#)].
- [67] L. D. McLerran, M. E. Shaposhnikov, N. Turok, and M. B. Voloshin, *Why the baryon asymmetry of the universe is approximately 10^{*-10}* , *Phys. Lett.* **B256** (1991) 477–483.
- [68] G. W. Anderson and L. J. Hall, *The Electroweak phase transition and baryogenesis*, *Phys. Rev.* **D45** (1992) 2685–2698.
- [69] A. Ahriche, *What is the Criterion for a Strong First Order Electroweak Phase Transition in Singlet Models?*, *Phys. Rev.* **D75** (2007) 083522, [[hep-ph/0701192](#)].
- [70] D. J. Chung and P. Zhou, *Gravity Waves as a Probe of Hubble Expansion Rate During An Electroweak Scale Phase Transition*, *Phys. Rev.* **D82** (2010) 024027, [[arXiv:1003.2462](#)].
- [71] S. J. Huber and T. Konstandin, *Gravitational Wave Production by Collisions: More Bubbles*, *JCAP* **0809** (2008) 022, [[arXiv:0806.1828](#)].

- [72] C. Caprini, R. Durrer, and G. Servant, *The stochastic gravitational wave background from turbulence and magnetic fields generated by a first-order phase transition*, *JCAP* **0912** (2009) 024, [[arXiv:0909.0622](#)]. * Brief entry *.
- [73] T. Kahniashvili, L. Kisslinger, and T. Stevens, *Gravitational Radiation Generated by Magnetic Fields in Cosmological Phase Transitions*, *Phys.Rev.* **D81** (2010) 023004, [[arXiv:0905.0643](#)].
- [74] S. R. Coleman and E. Weinberg, *Radiative Corrections as the Origin of Spontaneous Symmetry Breaking*, *Phys. Rev.* **D7** (1973) 1888–1910.
- [75] L. Dolan and R. Jackiw, *Symmetry Behavior at Finite Temperature*, *Phys. Rev.* **D9** (1974) 3320–3341.
- [76] R. Jackiw, *Functional evaluation of the effective potential*, *Phys. Rev.* **D9** (1974) 1686.
- [77] M. E. Carrington, *The Effective potential at finite temperature in the Standard Model*, *Phys. Rev.* **D45** (1992) 2933–2944.
- [78] C. Ford, D. R. T. Jones, P. W. Stephenson, and M. B. Einhorn, *The Effective potential and the renormalization group*, *Nucl. Phys.* **B395** (1993) 17–34, [[hep-lat/9210033](#)].
- [79] Amsler, C. et al (Particle Data Group), *Review of Particle Physics*, *Phys. Lett.* **B667** (2008) 1.
- [80] J. I. Kapusta, *Finite-Temperature Field Theory*. Cambridge University Press, The Pitt Building, Trumpington Street, Cambridge CB2 1RP, 1989.
- [81] J. A. Casas, J. R. Espinosa, M. Quiros, and A. Riotto, *The Lightest Higgs Boson Mass in the Minimal Supersymmetric Standard Model*, *Nucl. Phys.* **B436** (1995) 3–29, [[hep-ph/9407389](#)].